1

The Milky Way Galaxy

"I know not the true face of the mountain, for I am in its midst"
– Su Shi (1037-1101)

1.1 The Galaxy: seeing the forest for the trees

The Milky Way galaxy is the home of the Solar system and planet Earth, and yet we know disturbingly little regarding what it actually looks like. Simply by looking up into the night sky we observe the bright stream of stars and gas that is Milky Way, from which it is logical to assume the host of the Solar System is a flattened structure (see Figure 1.1). Such thoughts were postulated as early as the seventeenth century by Galileo Galilei, observing that the Milky Way actually consisted of numerous individual stars rather than a continuous "celestial fluid" (Binney & Merrifield 1998). Later work by Thomas Wright and Immanuel Kant in the eighteenth century developed this idea by proposing the Milky Way was effectively an upscale Solar System, with stellar bodies orbiting the central point on near-circular orbits, counter-acting the immense gravitational forces of the combined stellar stellar system. Kant also proposed that sources that were seen to be more nebulous and blurred out, rather than point like, could be analogues to our own Milky Way, or "island universes" (Kant 1755).

In the later eighteenth century Charles Messier and William Herschel undertook a systematic cataloguing and measuring of celestial sources. Herschel produced a diagram of the entire night's sky (right, Figure 1.2), including many more fuzzy nebulae (Herschel 1785), believing these were indeed island universes postulated by Kant as he was able to resolve discrete sources within them. Some of the first observations of spiral structure in the night sky were made by William Parsons, the Third Earl of Rosse, in 1845 using his appropriately named *Leviathan of*

Figure 1.1: Panoramic view of the Milky Way viewed from Earth. Credit: ESO/S. Brunier.

Parsonstown (Bailey et al. 2005), discovering nebulae both disc-like and spheroidal in nature, and clear spiral/whirlpool like patterns in nebulae such as M51 (left, Figure 1.2), adding further support to the notion that nebulae undergo large scale rotation.

In the early twentieth century a large global network of calibrators led by Jacobus Kapteyn employed the use of photographic plates and proper motions to produce a three-dimensional map of the Milky Way (Kapteyn 1922). Kapteyn proposed a disc-like Milky Way, 8kpc in radius, with a drop in stellar density towards the edges, with the Solar distance being only around 0.6kpc from the centre. The seemingly unlikely placement of the sun in the centre of the Milky Way was a troubling one. Kapteyn's measurements were undermined by the presence of an interstellar medium (ISM, specifically dust) that subdued the light from the Milky Way stars, thereby exaggerating their distances from the Earth. This caused a net preference for a strong drop off in stellar density from the Earth which could be misinterpreted as a heliocentric view of the Milky Way. Kapteyn's work also indicated the existence of two distinct stellar streams, i.e. that the motion of stars was not random, but rather moved in two streams moving in opposite directions, further endorsing the theory of Galactic rotation. Work around the same time by Harlow Shapley presented a radically different view of the Milky Way's structure based on distance measurements of globular star clusters and Cepheid variables (Shapley 1918a,b,c and other papers in this series). Shapley's analysis indicated that clusters were not uniformly distributed in the plane of the Milky Way, suggesting instead that the Solar System was significantly displaced from the centre, by some 15kpc, and that the Milky Way was nearly 100kpc in diameter. The Kapteyn and Shapley universes differed in many regards, both being the victims of the effect of inter-stellar absorption, the full importance of which was not quantified until the work of Trumpler (1930), who discovered that open stellar clusters at large distances were much fainter than they should be for their apparent size. This absorbing effect heavily undermines the distance determinations underpinning both Galactic models.

Shapley's ideas surrounding the structure of the Milky Way extended to those on external spiral nebulae, which he believed must be small constituent components of the Milky Way itself due its apparent huge size. This view was not accepted by all, with some preferring the smaller

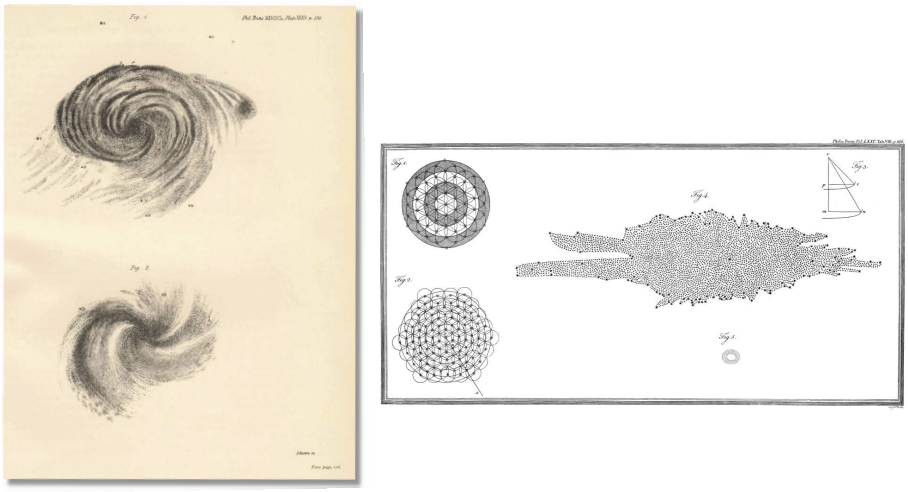

Figure 1.2: Left: sketches of M5 (top) and M99 (bottom) by Lord Rosse in 1850 from Bailey et al. (2005). Right: William Herschel's map of the Milky Way (Fig. 4 insert) from Herschel (1785). The Earth is located at the bright dot near the centre.

Kapteyn model of the Milky Way, with spiral nebulae existing as entirely separate entities. The conflicting models were pitted against each other at the so-called "Great Debate" in 1920, where Heber Curtis was given the challenge of standing for the "island universe" paradigm against Shapley, though there was no clear winner (Hoskin 1976).

In the advent of galactic spectroscopy it became apparent that nebulae shared very similar characteristics with stellar spectra, with full spectra that resembled that of the integrated Milky Way, backing the "island universe" view. Additionally, Doppler shifts gave the relative velocity of these systems, which seemed to be much higher than the stars in the plane of the Milky Way, further supporting the idea that nebulae were dynamically uncoupled to our Galaxy. Support for the Shapley model was hinged on a lack of knowledge about the absorbing properties of the ISM. He questioned if the Milky Way was like spiral nebulae, then why is it significantly darker and redder? Missing from the Shapley model was the absorbing ISM that has a tendency to absorb in the blue and would diminish the total luminosity of the galactic disc when viewed from the Earth.

The Great Debate was not truly settled until Edwin Hubble's observations in the mid 1920's. By resolving Cepheid variables inside these nebulae it was possible to determine their distances. It turned out they were far too distant to be considered part of the Milky Way itself and thus these collections of stars lying external to the Milky Way became known as galaxies. Around the same time efforts were also being made into measuring the kinematic properties of stars in the Milky Way. Bertil Lindblad and Jan Oort discerned that stars in the Solar vicinity are rotating in a highly flattened disc with velocities between 200-300 $\mathrm{km\,s^{-1}}$ (too high to remain bound in Kapteyn's smaller Milky Way).

Further insights into the structure of the Milky Way came from the discovery of the H I 21cm emission line (see Section 1.4), predicted by Hulst in 1941 and not seen until 1951 by a number of observers (see Binney & Merrifield 1998). This line was well separated from other spectral features, allowing for precise measurements of line-shifts. The biggest benefit of this line

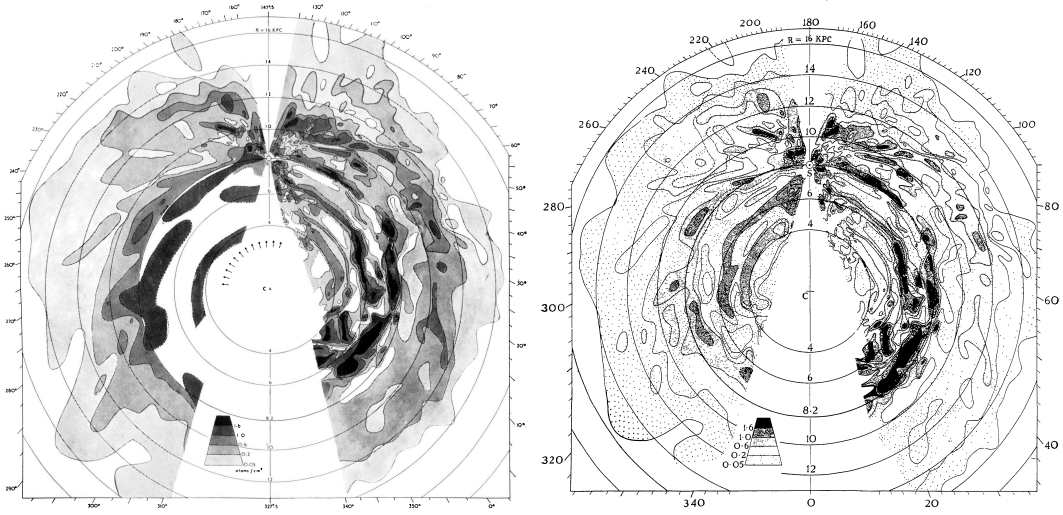

Figure 1.3: Top-down H I 21-cm emission maps of the Milky Way from Oort et al. (1958) on the left and Kerr (1962) on the right. The sun is located approximately two thirds from the bottom of each figure in the centre.

was its position in the radio regime, far from the dust absorption that hampered so many previous works, providing a tracer capable of mapping much deeper in the Galactic disc. This enabled Oort et al. (1958) to build a near-full map of the Galactic plane (left, Figure 1.3). Clearly the map is asymmetric, which could be a pointer towards spiral structure, but on average displayed a uniform density with azimuth. Note the over-abundance of material towards our Solar System, located approximately two-thirds up the y-axis. This is because the map assumes circular orbits, and spiral perturbations could cause non circularity giving the tendency of gas to point towards the observer. In later maps you can begin to see clearer spiral structure in the H I gas (Kerr 1962, right Figure 1.3).

The evidence outlined above leads to the categorisation of the Milky Way as a disc galaxy with net rotation and a diameter of 20-30kpc. However, inferring anything more concrete than this has been a point of contest for researchers for the past decades. While the existence of *some* spiral structure is widely undisputed, the exact morphology and kinematics are still shrouded in confusion. The problem is inherent to our position within the Galactic disc. As we lie within it there is no easy way to construct a full top-down map with irrefutable accuracy (and it is highly unlikely we will ever travel far enough out of it to do otherwise!). As can be seen from Figure 1.3, it is possible to infer some structure. However, the underlying calculations rely upon difficult distance determinations with large uncertainties and rely on some assumed rotation model. Even then, it is nigh impossible to apply these methods to behind the Galactic centre due to the extreme brightness in the entire electromagnetic (EM) spectrum.

The topic of this thesis is to constrain the morphology of the Milky Way through numerical simulations, reverse engineering them to reproduce observations seen here on Earth. Exactly how this is done will be discussed later in this Chapter, before which we will discuss some key points regarding galactic morphology and inter-stellar physics.

Figure 1.4: A collection of disc galaxies with clear morphological features. Top row from left to right shows three spiral galaxies; M51 (“Whirlpool”), M101 (“Pinwheel”) and NGC 4414. The bottom row shows three barred galaxies; UGC 12158, NGC 1672 and NGC 1300. Images credit; NASA, ESA, and The Hubble Heritage Team (STScI/AURA).

1.2 The galaxy zoo

Galaxies come in a whole host of morphologies, ranging from flattened spheroids to grand design spirals. They can generally be classified into one of three categories; disc, elliptical or irregular (the latter being anything that can’t be classified as the former). While the exact morphology is uncertain, our own Milky Way is generally accepted to be a multi-armed disc galaxy. Spiral armed galaxies are characterised by their winding arms, and often have an extended bar structure in the inner disc, from which arms can propagate. Figure 1.4 shows some of the more striking spiral galaxies observed by the Hubble telescope, with varying morphologies. M51 is the poster child for galactic spiral structure, whose arms are believed to have been produced by interaction with the nearby companion galaxy NGC 5195. The arms of M101 are less clearly defined and more numerous. NGC 4414 displays very flocculent spiral structure, with no distinct arm number. Three examples of barred galaxies are shown in the lower row of Figure 1.4, with arm morphology and inner gas/dust features. While NGC 1672 and NGC 1300 have a very dominant bar structure, UGC 12158 has only a weak inner bar, with multi-armed spiral features dominating the outer disc. Edwin Hubble attempted to classify these many different galaxies using a “tuning fork” diagram (Figure 1.5), where spiral galaxies are either classified as barred, SB, or unbarred, S (Hubble 1936). This is then followed by an index defining the features of the spiral pattern. Sa spirals have tightly wound arms, Sb intermediately wound arms and Sc very loosely wound arms. The size of the central bulge decreases from Sa to Sc. Sa spirals have poorly resolved arms and relatively little gas compared to the Sc’s (similarly for SB barred spirals). The actual number of spiral arms observed in external galaxies varies from 2-6, though as the number of arms increases the galaxies tend to be described as flocculent, showing arm-like features but either too disperse or too numerous to clearly quantify.

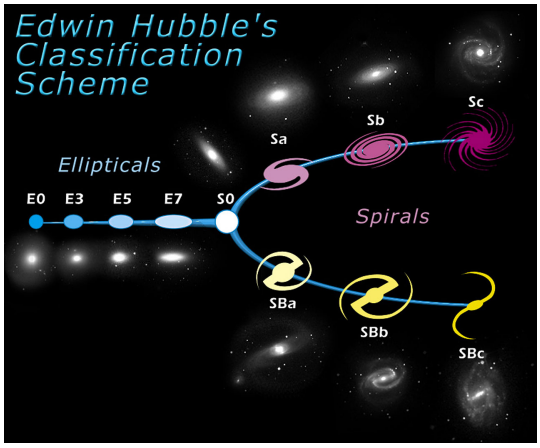

Figure 1.5: Hubble tuning fork diagram categorising the morphology of elliptical and spiral galaxies. Adapted from http://www.spacetelescope.org/images/heic9902o/ (credit: NASA and ESA).

While spiral galaxies form circular rotating discs, elliptical galaxies are spherically symmetric, oblate, prolate, or triaxial structures and have no clear surface patterns. The degree of spherical symmetry is categorised by the number of the elliptical, e.g. an E0 elliptical is completely spherically symmetric while an E7 is strongly prolate. The link between the elliptical and spiral classes is a lenticular class (or S0's), which are essentially spirals with no patterned features and a low gas content, though their exact relation between the elliptical and spiral galaxies is not entirely clear (see Sandage 2005 for a discussion). When studying the Hubble sequence one could be lead to the belief that the ellipticals evolved into the spirals over time, with the rotation flattening out the initially spherical stellar distribution into compact discs. This is however not the case, and no direct evolutionary path is implied by these classification schemes. "Early" and "late" type galaxies refers instead to evolution of morphological complexity in classification schemes (Binney & Merrifield 1998).

As well as their general outward morphology, elliptical and spiral galaxies have very different populations and internal structure. Elliptical galaxies are made up of much older stars (Population II[1]) with less ISM gas than spirals and as a result are redder in colour. The brightness decays slowly with radius by; $I(R) \propto \exp(-R^{0.25})$ (de Vaucouleurs 1948). The orbits of the stars inside the ellipticals are usually randomly orientated with no net rotation. If they are do exhibit a net rotation, it is slower than that in seen spirals.

Spiral galaxies on the other hand are mainly composed of Population I stars and have a large proportion of their mass in ISM gas and dust. They are often visually distinctive with their strong spirals emanating from the galactic centre with occasional bar like inner structures such as those in Figure 1.4 (see later in this chapter for more detail on the spiral and bar patterns). The surface brightness in the disc is characterised by an exponential drop off from the centre; $I(R) \propto \exp(-R)$, a steeper drop than that of Ellipticals (Freeman 1970; Binney & Tremaine 1987). Spiral galaxies tend to have a spherical inner nucleus, known as a bulge, which is very similar to

[1]Stars can generally be classified as either Population I or II. The former are young, hot, metal rich stars found in galactic discs. The latter are cooler, metal poor, often late in age and are found in globular star clusters.

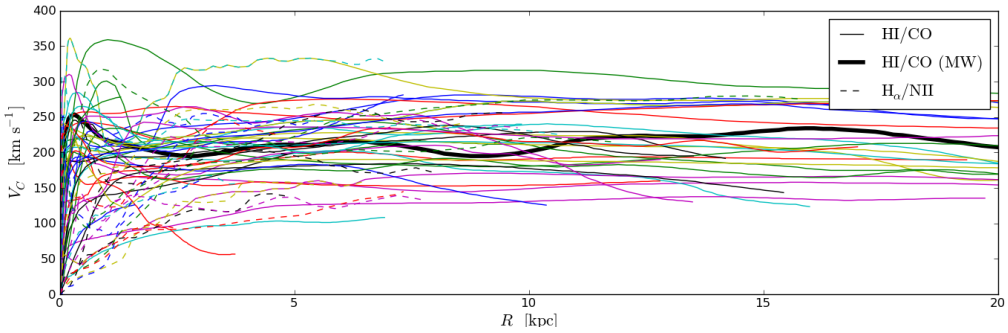

Figure 1.6: A selection of rotation curves from (Sofue & Rubin 2001) for spiral 52 spiral galaxies including the Milky Way (thick black line). Data is either from the CO 2.6mm, H I 21cm, H_α 656nm and N II 122μm emission lines.

a small elliptical galaxy. The bulge has random rotation and is composed of mostly Population II stars with little ISM gas and dust. The velocity distribution of the stars inside the disc tends to be roughly flat with radius; the rotation of spiral galaxies is constant as you move away from the galactic centre. Figure 1.6 shows the rotation curves for 52 spiral galaxies using a variety of different data sources from Sofue & Rubin (2001), showing flat rotation in most cases. The flat nature of the disc galaxy rotation curves presented a problem for galactic mass determinations, and is in many ways still an unsolved problem even in the 80 years since its first detection by Oort (1932). If the stars in galaxies were to orbit like objects in our own Solar System then they should obey Kepler's third law. That is, the orbital period should increase, and the speed decrease, as you move away from the galactic centre (the blue line in the left panel of Fig. 1.7). If it were a solid body-like rotation then velocity would have to increase as you move from the larger radii to stop the disc form breaking apart. However, studies began to show that galaxies had neither Keplarian nor solid body rotation. This is seemingly at odds with the luminosity profiles of disc galaxies, which clearly decay with increasing radii, indicating some material was contributing to the mass of the system but not to the luminosity. Evidence of so-called "dark matter" was seen in observations of individual stars (Rubin et al. 1980), galaxy clusters (Zwicky 1933), individual galaxies (Ostriker et al. 1974) and also in elliptical and dwarf galaxies (see the review of Trimble 1987 for a full discussion of evidence).

However, this dark matter has still yet to be observed in any direct way due to its indifference towards all regions of the EM spectrum. Figure 1.7 shows rotation curve measurements for the Milky Way from Sofue (2012). In the right panel a combination of an inner bulge and disc cannot reproduce a flat curve without some extra outer mass component. By including a spherically symmetric outer massive halo the rotation curve can then be flattened. The matter needed to do this, regardless of geometry of the halo, would imply that dark matter would outweigh regular matter by nearly an order of magnitude (Fich & Tremaine 1991; Battaglia et al. 2005). The spatial distribution of the dark matter is often assumed to be spherical, though the exact morphology is yet another unkown. Even 30 years after its original postulation, we can tell little more about dark matter other than the gravitational force it exerts.

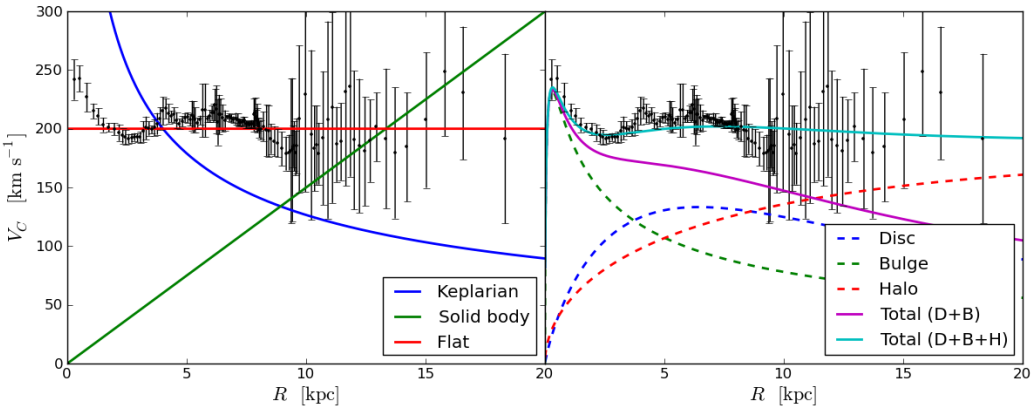

Figure 1.7: Left: rotation curve data for the Galaxy from Sofue (2012) with a Keplarian, solid body and flat model curve. Right: The same data with a flat model curve reproduced from combining a circular disc, spheroidal bulge and spherical halo of material.

1.3 Spiral and bar structure

While spiral patterns appear in no short supply in disc galaxies, upon first discovery there was considerable confusion as to what the underlying physics was behind them. One of the biggest conundrums was why the spirals were seen at all. If disc galaxies had flat rotation curves (as most do, see Fig. 1.6), then any pattern seen on the disc would not stay the same as the disc rotated (see the solid body curve in Fig. 1.7). For a flat rotation curve rotation frequency scales as $\Omega \propto 1/R$, and so the inside of an observed pattern would move at a much faster angular speed than the pattern at large radii. This effect, known as the "winding problem", meant that any spiral pattern would wind up into nothing after a few galactic rotations, and yet many disc galaxies at various redshifts are seen to have strong spiral features, indicating that galaxies either maintained their spirality or continuously reformed spiral arms.

Some of the earliest advances in understanding spiral structure were made by Lindblad in the early twentieth century. Lindblad developed the idea that spiral structure resulted from stellar and gaseous gravitational interactions during their orbits around the galactic centre. His idea was that spiral structure was seeded by leading spiral arms born at the edge of the stellar disc, with eccentric stellar orbits driving $m = 2$ spiral modes. Lindblad's work was underpinned by his theories of stellar orbits, which became a mainstay of future spiral models (see Pasha 2004a and Pasha 2004b for a review of Lindblad and early spiral structure theory). Consider stars/gas moving in some axisymmetric potential, such as that of a disc galaxy, in a near-circular orbit at a frequency of Ω. The equations of motion of the material are given by those of a circular orbit with perturbing terms; $R(t) = R_g + r'(t)$ and $\theta(t) = \Omega t + \theta'(t)$ where R_g is the average radius of the nearly circular orbit with $r'(t)$ and $\theta(t)'$ the deviations from a circular orbit in the radial and azimuthal directions respectively. The resulting equations of motion for the radial offset is $\ddot{r}' = -\kappa^2 r'$ (see Combes et al. 1995 for a derivation). As the equation of motion is only solved to first order this is known as the *epicycle approximation*. The frequency of radial oscillation, κ, is referred to as the epicycle

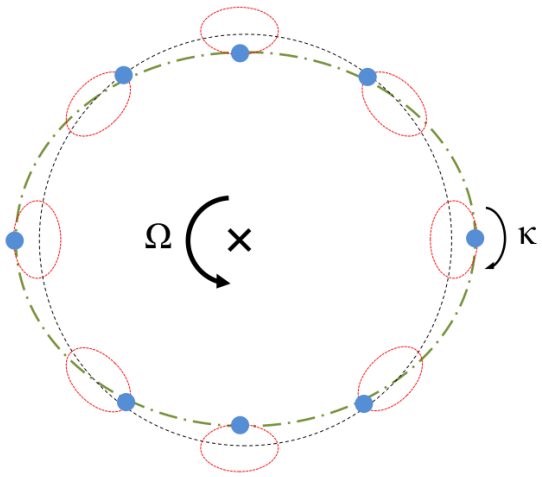

Figure 1.8: The orbital path of a star (blue dot) around the galactic centre with epicycle frequency of $\kappa = 2\Omega$. The epicycle, circular and resulting full orbital path are shown by the red, black and green lines.

frequency, and is given by

$$\kappa^2 = \frac{\partial^2 \Phi_{\rm axs}}{\partial R} + 3\Omega^2 \equiv R\frac{{\rm d}\Omega^2}{{\rm d}R} + 4\Omega^2 \equiv \frac{2\Omega}{R}\frac{\rm d}{{\rm d}R}R^2\Omega, \tag{1.1}$$

where $\Phi_{\rm axs}$ is the axisymmetric potential of the stellar system. While orbiting the galactic centre at Ω, the star is also rotating in a small ellipse in the rotating reference frame with radial frequency κ, where the combined orbit has the general shape of a rosette. The magnitude of κ is dependent on the rotation curve. For example, in the galactic centre the rotation curve is as a solid body, $V_c \propto R$, and so $\kappa = 2\Omega$. In the outer disc the rotation is differential, $V_c = $ const., so $\kappa = \sqrt{2}$. In general, $\Omega < \kappa < 2\Omega$, so the material completes an epicycle before it completes a full orbit. Figure 1.8 shows a star orbiting the galactic centre with an epicycle frequency of $\kappa = 2\Omega$, and the resulting effectively elliptical closed orbit.

The shortcomings of spiral models to fully solve the winding problem led to the postulation in the 1950's that large scale magnetic fields were the driving force of spiral structure. Observations of the field strengths in galaxies however indicated that field strengths were simply too weak to be responsible for large scale arm features (see Binney & Tremaine 1987).

1.3.1 Density wave theory

The work of Lindblad lead to one of the most popular theories of spiral structure. The spiral density wave theory of Lin & Shu (1964) formulated the spiral features not as a specific collection of stars, but rather a density wave that propagates azimuthally through the galactic disc. The spiral arms would manifest as over-densities in the stellar population, with stars passing into and then out of the density wave rather than spending their entire lifetimes within the arm. An often used analogy is that of a traffic jam on a road. Cars enter and leave the traffic jam, creating an over-density in cars at a certain point. The jam is still moving, albeit at a different speed to the cars,

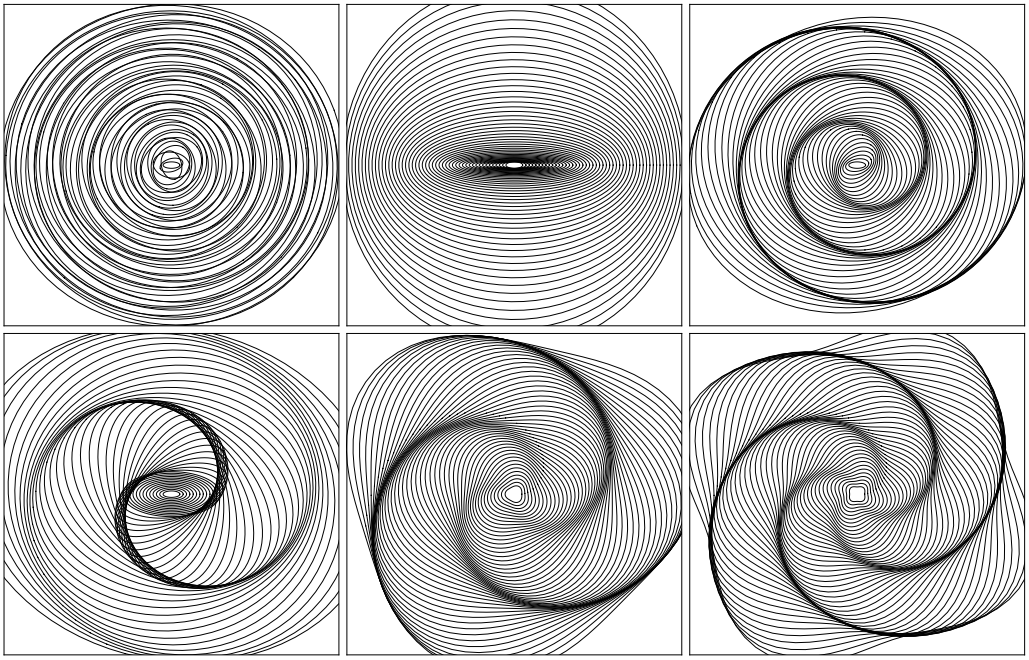

Figure 1.9: Illustration of the how the superposition of numerous stellar orbits can create bar and spiral patterns. Top left shows that random alignments of elliptical orbits creates no pattern, resulting in disc only structures. Top centre is a continuous superposition of ellipses aligned horizontally, creating a bar-like inner structure. The spiral pattern in the top right is made by simply incrementing the offset of each orbit steadily with increasing semi-major axis. Bottom left is a combination of a bar and 2 armed spiral through a simple combination of ellipses. The 3 and 4 armed spirals require non-elliptical orbits and for the masses to complete 3 or 4 complete radial oscillations during a full orbit (3/1 or 4/1 opposed to an ellipse's 2/1).

which enter and leave the jam over time. In this sense the traffic jam is a density wave, and cars do not reside in a single jam forever. With a steady spiral density wave it is possible to create any number of arm or bar structures, to have both leading and trailing arms, and avoid the winding problem.

The resulting stellar perturbation caused by this density wave is represented as a surface density of the form[2]

$$\Sigma_{sp}(R, \phi, t) = A_{sp}(R) \cos\left[m\phi + f(R) + \Omega_p t\right] \tag{1.2}$$

where A_{sp} defines the spiral radial strength, m the order of the spiral (i.e. number of arms), Ω_p the rotation frequency of the density wave and $f(R)$ the *shape function* of the arms. The shape function defines the morphology of the arms, whether it be a logarithmic, Archimedean, or hyperbolic spiral. The most common shape function is that of a logarithmic spiral, which has the form

$$f(R) = \ln(r/r_\circ)\cot(\alpha) \tag{1.3}$$

where $r_\circ$ is some constant and α is the pitch angle; the angle the arm makes with a tangent to a

[2]This can also be expressed as $\exp(i[m\phi + f(R) + \Omega t])$.

circle of constant radius. An example of how these spirals relate to actual stellar orbits is shown in Figure 1.9 (based on a similar diagram of Kalnajs 1973). In the first panel we show a set of elliptical orbits, closed such that $\kappa = 2\Omega$. The orbits are randomly rotated with radii, showing no distinct pattern. In the second panel we leave all orbits aligned with the x-axis, forming a bar-like feature in the inner disc. By then rotating each orbit with increasing radius we can form spiral patterns similar to those seen in disc galaxies. Multi-arm structures can be created by increasing the epicycle frequency, e.g. $\kappa = 3\Omega$ (or $\kappa = 3\Omega/2$) and $\kappa = 4\Omega$, creating 3 and 4 armed spiral patterns.

A dispersion relation for the spiral structure can also be formulated, but depends on a few key assumptions. The spiral must be sufficiently tightly wound. This simplifies the computation of long range gravitational forces in the disc, as it ensures there is some local density perturbation providing the majority of the gravitational force[3]. The spirals are also assumed to rotate as a rigid body and do not deform in shape over time (Ω_p and α are constant). The arms are said to be quasi-stationary spiral structures; QSSS (Dobbs & Baba 2014). This results in a dispersion relation of the form

$$(\omega - m\Omega)^2 = \kappa^2 - 2\pi G\Sigma|k| \tag{1.4}$$

where k is the radial wavenumber of the spiral density wave, ω is its angular frequency and Σ the surface density of the disc (Toomre 1964). The dispersion relation for a hot gas disc (the above is for a cold gas disc) was provided by Lin & Shu (1964) and requires an additional term of $c_s^2k^2$ added to the RHS of Equation 1.4, where c_s is the sound speed of the gas. A stellar dispersion relation is similar also to Equation 1.4, except with an additional multiplication factor added to the Σ term which is a summation of Bessel functions of Ω, ω, κ, k and the radial velocity dispersion of the stars, σ (Kalnajs 1965; Lin & Shu 1966). The pattern speed is related to the arm angular frequency by $\omega = m\Omega_p$. From these dispersion relations two key stability criteria can be found, referred to as Toomre Q parameters. If the terms on the RHS of Equation 1.4 are > 0 then a solution exists where Ω_p is real, and hence Equation 1.2 holds and the disc is stable. If, however, the LHS of Equation 1.4 is < 0 then Ω_p is complex, and Equation 1.2 will then contain an exponentially increasing factor, hence making the disc unstable (Binney & Tremaine 1987; Dobbs & Baba 2014). By extension to warm stellar and gaseous discs the respective Q parameters can be defined as

$$Q_g = \frac{\kappa c_s}{\pi G\Sigma} \tag{1.5}$$

and

$$Q_s = \frac{\kappa\sigma}{3.36G\Sigma}. \tag{1.6}$$

Stability of the discs requires $Q > 1$, and instability is present when $Q < 1$. Physically, Q can be thought of as the balance between the disc pressure forces (driven by velocity dispersion in stars or thermal dispersion in gas) and gravitational attraction of the disc of surface density Σ. Values in the Solar neighbourhood are approximately $Q_s \approx 2.7$ and $Q_g \approx 1.5$ implying the Solar neighbourhood is stable, but not by a large margin in the gas (Binney & Tremaine 1987).

There exists some regions of special interest when considering Equation 1.4. When epicycle

[3]This is also referred to the tight-winding, or WKB, approximation (Binney & Tremaine 1987).

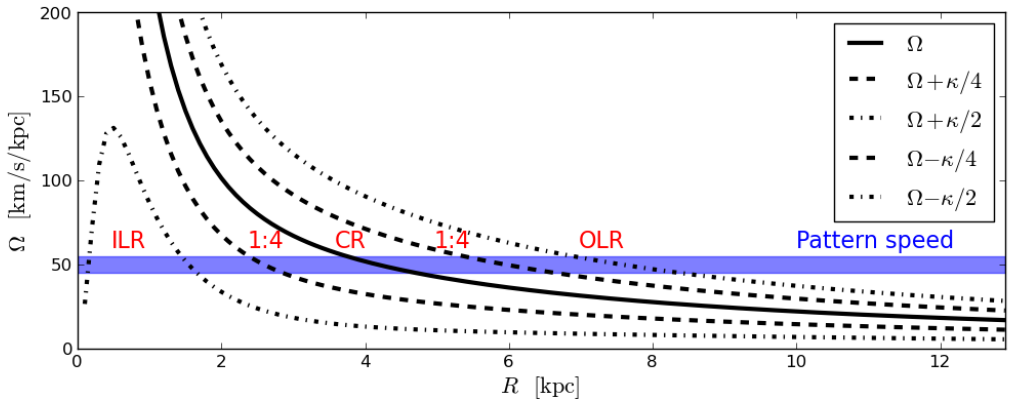

Figure 1.10: Rotation speeds for a Milky Way-like rotation curve. The dashed and dot-dashed lines show the 4:1 and 2:1 resonances calculated from the epicycle frequency, κ. The shaded region shows the the location of the pattern speed, which is in keeping with that of the Milky Way bar.

orbits close as some fraction of the orbital frequency we obtain the relation

$$\Omega - \Omega_p = \pm\frac{\kappa}{m} \tag{1.7}$$

where m is some integer, representing the number of arms. This equation is only satisfied at two radii for each m which are known as the inner and outer Lindblad resonances (ILR and OLR), usually defined with reference to $m = 2$. At the ILR and OLR the orbiting material orbits such that it encounters the density wave at the same point in the orbit each rotation, and experiences a resonance as a result. There also exists an intermediate radius where $\Omega = \Omega_p$, the co-rotation radius (CR). At the ILR the material moves faster than the perturbation, with the perturbation at CR, and slower than it at the OLR. Some examples of these different resonances are shown in Figure 1.10, where the ILR, OLR, and CR are shown for a Milky Way like rotation curve. The shaded region shows the pattern speed of some imposed perturbing density wave ($\Omega_p = 50\mathrm{km\,s^{-1}\,kpc^{-1}}$, which is closer to the bar pattern speed than that of the arms, but the principle is the same). Where Ω_p crosses the different resonant lines $\Omega \pm \kappa/m$ dictates the location of the resonance features. In this example there are actually two ILR due to the shape of the rotation curve near the galactic centre caused by the bulge.

The waves described by the dispersion relation above will in fact migrate radially, at some group velocity given by

$$v_g = \frac{\mathrm{d}\omega(k)}{\mathrm{d}k} = \pm\frac{|k|c_s^2 - \pi G\Sigma}{m(\Omega_p - \Omega)} \tag{1.8}$$

first formulated by Toomre (1969). As waves propagating radially they reverse direction when they come close to the CR, as k decreases R increases and vice-versa, and are reflected (or damped[4]) when they approach the Lindblad resonances. Density waves are thus not permitted to pass the

[4]Damping at the ILR can be reduced, and transformed into reflection if Q increases significantly at the ILR, creating a so-called Q-barrier. This is believed to occur in the Milky Way, and a Q barrier is seen in our calculations in Chapter 5.

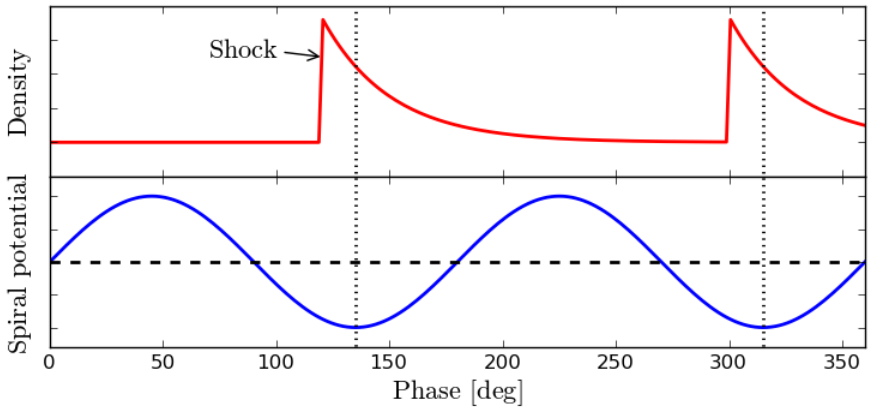

Figure 1.11: Position of ISM shock (top) resulting from passage into spiral potential (2-armed, bottom). The position of the shock, signified by compression and increase in density, is offset from the bottom of the spiral potential well. Based upon work by Roberts (1969).

ILR and OLR, where a build up or reflection of wave packets occurs (see Binney & Tremaine 1987, Combes et al. 1995 and Dobbs & Baba 2014 for further details). As a result of a non-zero group velocity, the wavenumber increases. This causes a tightly wound trailing wave to unwind, and eventually transition into a loose leading wave, which then winds up. The winding is much slower than material arms, but still presented a problem for theorists, as the whole point of density waves is that they are supposed to not be susceptible to the winding problem.

As density waves can be propagated through the disc, and as a result be dissipated over time, systems of re-seeding density waves need to be present. Such a solution is the theory of "swing amplification", which will be discussed in Section 1.3.2.

Spiral shocks

Soon after models of spiral structure emerged, theories of the spirals effect on the interstellar gas also surfaced. Galaxies such as NGC 5383 and M81 display striking dust lanes aligned along their spiral arms, suggesting compression of gas/dust caused by shocks induced by the spiral density waves. Fujimoto (1968) and Roberts (1969) postulated that a supersonic gas flow into a spiral density wave experiences a shock as a result of the rapid deceleration. This would occur *before* reaching the spiral minima, shown in Figure 1.11, and gas would accelerate once more as it leaves the arm/shock and travels towards the next. The sudden compression of gas at these spiral shocks is theorised to act as a trigger for star formation due to the accumulation of molecular gas in regions of high density. Young stars will then be seen to trail the spiral potential, as will ionised H II regions.

The offset of the peak gas and stellar densities as shown in Fig. 1.11 is not universally accepted however. Wada et al. (2011a) and Dobbs & Bonnell (2008) find that gas shocks do not appear to be offset from the stellar spiral potential well in calculations with dynamic stellar spiral potentials, where the structures are not long-lived, and so gas will develop with the arm and travel with it, rather than traverse through a well established density wave. Conversely, calculations

with fixed potentials tend to observe offsets between spiral minima and ISM shocks (Yuan & Grosbol 1981), though not always necessarily leading the arm (Gittins & Clarke 2004; Elmegreen & Thomasson 1993).

The actual response of ISM gas to a spiral perturbation is much more complex than a single shock front leading the arms. Numerical simulations including ISM heating and cooling show instabilities and shock fronts that are no means uniform across the arms (Shetty & Ostriker 2006; Wada 2008; Dobbs et al. 2008; Smith et al. 2014). This non-uniform response creates spurs and feathering features trailing from the spiral arms[5]. Wada & Koda (2004) believe these features are caused by a 'Wiggle-instability', essentially a manifestation of the Kelvin-Helmholtz instability, while Dobbs et al. (2008) theorise that they are simply caused by the amplification of cloud-scale substructures as they pass into the spiral shock.

1.3.2 Flocculent/dynamic spirals

While the density wave theory does solve some standing issues for galactic spirality, there is one major caveat. Thus far no direct evidence, be it observational or numerical, has been able to confirm the theory. Spiral arms can be seen in numerical simulations, but they are not persistent, rather transient and recurrent (see Sellwood 2011 for a review of spiral longevity). Material populates these arms for the lifetime of the arm itself, rather than flowing into and out of the perturbation as in density wave theory (see Wada et al. 2011b; Baba et al. 2013; Grand et al. 2013). Spiral arms in N-body simulations have two key differences to those of the density wave theory. They are material in nature, rather than propagating density waves, and they are recurrent, being victim to the winding problem. As the disc rotates the arms become sheared apart as they wind up, only for them to join different arm structures formed in their wake. While some authors find long lasting modes (e.g. Sellwood & Carlberg 2014), these arms are still transient with no fixed pattern speed. Arm features tend to only recur for a certain time, after which the disc tends to become featureless, or strongly barred (see Section 1.3.4). As the system evolves from initialisation, Q rises making the disc more stable to perturbations, eventually leading to the dissipation of spiral features (Sellwood & Carlberg 1984). The loss of spirality is even more severe with lower number of particles, implying it may also be a resolution effect (Fujii et al. 2011).

A key mechanism for generating these spiral features is "swing amplification". Numerical simulations of Toomre (1981) showed that a leading wavepacket could become significantly amplified as it transforms into a trailing wave and back into a leading wave. The transient trailing wave is even stronger still than the final leading wave, creating an amplification effect (Binney & Tremaine 1987). In order to set this swing amplification mechanism the initial leading spiral wave must be generated. Certain mechanisms for this have been theorised, such as a lack of ILR or reflection of density waves from a hard edge of the disc, though neither of these are likely in

[5]The terms branches, feathers and spurs are used interchangeably in the literature, but here we adopt the convention of Dobbs & Baba (2014). Branches are long, secondary arm features, resulting from bifurcation (e.g. the Local Arm in the Milky Way). Spurs and feathers and morphologically similar, which are smaller scale and more numerous, inter-arm features. Some define spurs as the star formation sites, and feathers as the dust lanes. In the work in this thesis there is no distinction between the latter two due to a resolution lacking to model star formation, and so we use spur and feather interchangeably.

the Milky Way (see Binney & Tremaine 1987 for a discussion). Swing amplification could also be responsible for the seemingly easy creation of bars in numerical simulations (Combes & Sanders 1981; Sparke & Sellwood 1987; Raha et al. 1991; Baba et al. 2009; Shen et al. 2010). See Chapter 5 for some examples of this phenomenon in our work.

The dominant mode of the swing-amplified spiral pattern is given by

$$m = \frac{\kappa^2 R}{2\pi G \Sigma X} \approx \frac{\kappa^2 R}{4\pi G \Sigma} \tag{1.9}$$

where $1 < X < 2$ generates spiral features, and $X = 2$ is a nominally adopted value (Fujii et al. 2011; Dobbs & Baba 2014). Equation 1.9 shows that the number of spiral arms is a strong function of the disc mass, with systems with high disc-to-halo mass ratios forming only a few strong spiral arms, whereas low mass discs form numerous but weaker arms (Carlberg & Freedman 1985). The dominant arm mode is also directly coupled to the Q parameter (Equation 1.6), and so seeding a disc with a very low Q will lower the expected m. Equation 1.9 only predicts the dominant mode, and any single simulation will have other spiral modes of comparable strength, and even then the dominant mode will increase with radius.

Further details on this mechanism of spiral formation will be presented in Chapter 5 where we show calculations using N-body stellar systems and their effect on the molecular content of the ISM.

1.3.3 Perturber/tidal induced spirals

The interaction between a galactic disc and some companion object can also seed arm structure. The poster child of spiral structure, M51 (top left, Fig. 1.4), is believed to have been seeded by such an encounter. Other notable examples include the Mice and Antennae galaxies, NGC 2207, and even our own Milky Way to a minor extent with the nearby L/SMC (Purcell et al. 2011). Encounters of this form drive bimodality in the disc at large distances, with severe disruption occurring as the companion nears the edge of the host (Combes et al. 1995). The attraction of the companion elongates orbits, effectively driving an epicyclic oscillation, which in turn will wind up due to the disc rotation creating spiral structures. These arms do not even require self-gravity in the stellar disc to become apparent, but it is required to ensure the tidal features are propagated to the centre of the disc as in M51 (Toomre 1981). Galactic tides may also be responsible in some part for disc warps, with the Milky Way's warp at $R > 9$kpc caused by the nearby L/SMC (Kalberla & Kerp 2009).

One of the first in depth simulations of interacting galaxies was performed by Toomre & Toomre (1972)[6]. Using only 120 particles the authors showed the relative ease of reproducing arm features (bridges, features connecting bodies, and tails, features approximately 180° offset to bridges). An example of these is shown in Fig. 1.12 where a companion, 1/4 the mass of the host galaxy, approaches on a parabolic orbit, distorting the disc into arm features similar to Arp 82,

[6]Worth mentioning is the study by Holmberg (1941), who "simulated" the interaction between two galaxies using lightbulbs, where the amount of light at any point represented the gravitational field of the combined galaxy system. Photocells measured the intensity of the light (which obeyed a $1/r^2$ law as gravity does), which was used to update the gravitational forces.

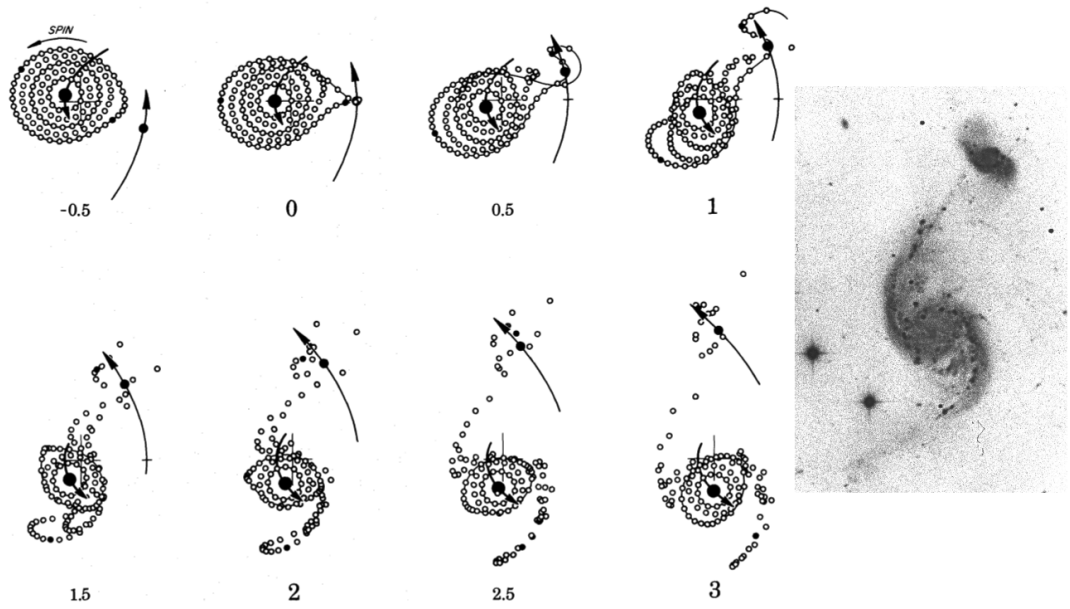

Figure 1.12: Interaction of a point mass companion with an N-body disc adapted from Figure 4 of Toomre & Toomre (1972). The initial perturber trajectory is parabolic with a mass 25% that of the primary galaxy, and the system is shown evolving in time from -0.5 to 3 in units of 100Myr (0 being perigalacticon passage). Clear bridge and tail features can be seen caused by gravitational attraction with the perturber. The right insert shows the Arp 82 system (a.k.a NGC 2535 and NGC 2536) from Arp (1966) showing similar tidal features.

shown in the insert.

The structures formed by these interactions are a mix of kinematic density waves (self-gravity in the stars is not required, Ω_p not fixed but winding slower than material arms), material waves (arms flow with the disc, $\Omega_p = \Omega(R)$), and density waves as in Section 1.3.1 (Ω_p = const.). The tails and bridges tend to be material arms and dissipate rapidly. Arms formed in simulations tend to have a pattern speed decreasing with radius, and are subject to winding up over time (Oh et al. 2008; Dobbs et al. 2010; Struck et al. 2011). Many examples now exist in the literature of tidally induced spirals, predominantly of the $m = 2$ mode (Elmegreen et al. 1991; Barnes 1992; Barnes & Hernquist 1996; Oh et al. 2008; Dobbs et al. 2010; Purcell et al. 2011; Struck et al. 2011). These successfully reproduce many observed galactic tidal encounters and computational resources are sufficient to also track the gas evolution, and the effect of a companion with an extended mass distribution.

1.3.4 Bar structure

Bars exist in many observed disc galaxies, as abundant as 30-50% (Binney & Tremaine 1987), being composed predominately of the old and red stellar population. They either dominate the disc structure as in NGC 1300 (SB class) or only extending to intermediate radii as in UGC 12158 (SAB class) or our own Milky Way. The bars themselves vary in dimensions, but are often very elongated and quite dissimilar morphologically to elliptical galaxies with axis ratios ranging from

Figure 1.13: Boxy/peanut bulges in the disc galaxies of Hickson Compact Group 87 (Credit: The Hubble Heritage Team, AURA/STScI/NASA, top) and NGC 5746 (credit: Palomar DSS, bottom).

2:1 to 5:1 (Combes et al. 1995). While ellipticals have a strong surface brightness drop-off away from their centre, bars have a near-constant surface brightness across their length. The vertical structure of bars is harder to assess, due to the difficulty in identifying bars in discs orientated edge-on. Numerical simulations suggest that a barred galaxy will display a boxy, or peanut, shaped bulge with lobes corresponding to the ends of the bar. Two examples of galaxies with such bulges are shown in Figure 1.13. Elliptical bulges are then either bar-free, or have a bar along the line-of-sight (Binney & Merrifield 1998).

While the density wave theory has had no irrefutable evidence supporting a single fixed pattern speed for the spiral arms, the pattern speed of bars does appear constant in simulations. The pattern speed of the bar is encompassed by the parameter $\mathcal{R}$, which relates the bar major axis to co-rotation radius, $R_{\rm CR}$, by

$$\mathcal{R} = R_{\rm CR}/a \tag{1.10}$$

where "slow" bars are defined by $\mathcal{R} \gg 1$ and "fast" bars have $\mathcal{R} \approx 1$. The co-rotation radius is in turn directly coupled to the pattern speed of the bar, and the pattern speed can be either measured directly using methods such as that of Tremaine & Weinberg (1984), or by comparison with simulations. The co-rotation and major axis of the bars follow a linear slope in many barred galaxies, with $0.9 < \mathcal{R} < 1.3$, and lie near $\mathcal{R} \approx 1$ within errors, making observed bars "fast" rotators (Binney & Tremaine 1987).

The equivalent equipotential surface of a simple barred gravitational potential is shown in the left panel of Figure 1.14 (i.e. in a reference frame rotating at the bar pattern speed; $\Phi_{eq} = \Phi_{bar} - \Omega_p^2 R^2/2$). There are five Lagrangian points; one at the centre, two unstable saddle points (red crosses) and two maxima (green crosses). Stars can oscillate around the maxima points at κ, and all the Lagrangian points combined outline the coronation zone (Combes et al. 1995). In the right panel of Fig. 1.14 the orbits in such a potential are shown, calculated by Contopoulos & Papayannopoulos (1980), showing several interesting features. At the centre of the bar a set of

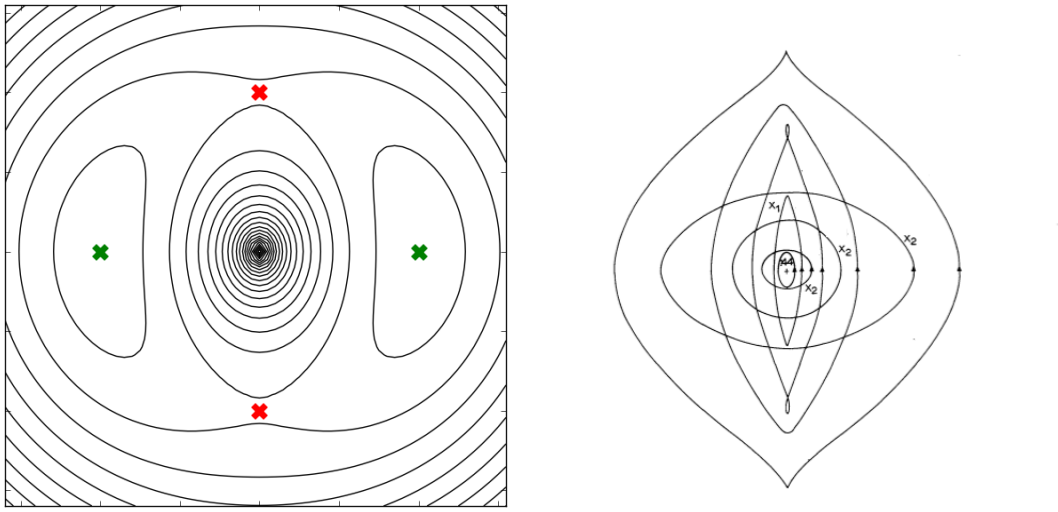

Figure 1.14: Left; orbits inside a simple biaxial potential representing a bar, from Binney & Tremaine (1987). Right; stable orbits inside such a potential, taken from Contopoulos & Papayannopoulos (1980). The bar is aligned vertically in both cases.

orbits parallel to the bar exist, denoted x_1 orbits. Beyond the CR the x_1 orbits now display lobes at their extremities. These orbits form the majority of the bar structure itself due to their stability and presence inside the CR. The x_2 family of orbits exist *perpendicular* to the bar major axis, and only exist between ILRs if they exist, which may not be the case for some disc structures. A further set of orbits exist around the lobe Lagrangian points (green crosses), that do not orbit the bar's centre. Well outside the CR orbits become circular again.

The above holds primarily for weak bars. For the strong case (SB class) orbits lie effectively only on the x_1 family (Contopoulos & Papayannopoulos 1980; Athanassoula 1992a). Modelling the orbits in these bars is more difficult, and they are usually studied via numerical simulations of unstable discs (Sparke & Sellwood 1987).

Numerical simulations have shown that while steady spiral structures are difficult to maintain, stable bars are easily created (e.g. Ostriker & Peebles 1973; Sparke & Sellwood 1987; Combes et al. 1990; Baba et al. 2009; Shen et al. 2010; Grand et al. 2012). The problem is not so much how to form bars, but rather how to hinder their formation to reproduce spiral galaxies with no bar component. The easiest way is to simply raise the stability of the disc by raising Q_s, which is easiest done by lowering the the disc to halo mass ratio, which also suppresses the swing amplification that helps further enforce the bar. A second way of suppressing bar formation is by ensuring the rotation curve has an ILR. As described in the previous section, an ILR stops trailing waves passing through the centre and forming leading waves on the opposite side of the disc (hence why arms are only formed outside of the ILR). While flat rotation curves are common in disc galaxies, this does not ensure an ILR, but the inclusion of a large central concentration will do (i.e. a bulge, as in Fig. 1.10). A criterion for bar formation was found by Efstathiou et al. (1982) of the form

$$\epsilon_b = \frac{V_{\max}}{\sqrt{GM_d/R_d}} \tag{1.11}$$

where $V_{\max}$ is the maximum velocity of the full rotation curve, M_d and R_d are the disc mass and scale-length respectively with bar formation requiring $\epsilon < 1.1$.

Bars are seen to have strong dust/gas lanes lying along either major axis, and often only on the leading side (see NGC 1300 in Fig. 1.4). The offset of these lanes to the bar itself, and their degree of curvature, is a related to the $\mathcal{R}$ parameter (Athanassoula 1992b). These then wind up near the galactic centre, forming nuclear rings around the central bulge. This transport of material results in a net gain of gas to the galactic centre, and accumulates at the inner x_2 orbits inside the outer ILR (Binney & Tremaine 1987). Star formation is seen at the bar ends rather than these parallel dust lanes, and bar ends are also the site of high density enhancements in simulations (Athanassoula 1992b).

Bar induced spiral arms

Bar and spiral arms often come hand in hand in nature, with $m = 2$ spirals extending from the ends of the inner bar. How and why the bar and spiral features are coupled is not clear, i.e. whether they inherently result from the same mechanism with identical pattern speeds, or whether they are dynamically separate entities. For instance, there is evidence that the bar and spiral features in our Galaxy have very different pattern speeds with the bar rotating at least twice the speed of the arms (see Gerhard 2011 and references therein). In the case where bars and arms share the same pattern speed, the arms trail directly off the bar ends and extend out to the OLR of the bar. These arms are seen in many numerical simulations of gas responding to some barred potential (Athanassoula 1992b; Englmaier & Gerhard 1999; Patsis & Athanassoula 2000; Wada & Koda 2001; Rodriguez-Fernandez & Combes 2008; Mel'Nik & Rautiainen 2009). While stellar orbits lie either parallel or perpendicular to a bar, the dissipative forces experienced by the gas allow for offset elliptical orbits caused by bar rotation. This causes orbits to trail, creating spiral arms in the gas emanating from the bar ends (Dobbs & Baba 2014). Eventually these arms in the gas will wind up to form rings at the OLR after the order 10 bar rotations (Schwarz 1981; Mel'Nik & Rautiainen 2009). Gas is evacuated from the CR region and is migrated to the ILR and OLR features. Having outer rings is not uncommon in observed galaxies (M95, NGC 1291), and neither are galaxies with arms transitioning into rings similar to those seen in simulations (NGC 3504, NGC 7479). The fact that all observed barred galaxies do not have outer rings indicates that the time-scale for bar formation and arm winding is of order of the age of the universe (Combes et al. 1995). There is some, though not much, evidence for decoupled arm and bar features in simulations, namely Sellwood & Sparke (1988) and Rautiainen & Salo (1999). Sellwood & Sparke (1988) find two distinct pattern speeds in their simulations, and observe the bar and arm features to disconnect and reform during rotation. Rautiainen & Salo (1999) find two different pattern speeds in *some* of their calculations, but not all, finding a decoupling that is epoch dependent. Grand et al. (2012) find distinct bar and spiral pattern speeds, but the arms are effectively material and rotate with the disc (having $\Omega_p \propto R^{-1}$).

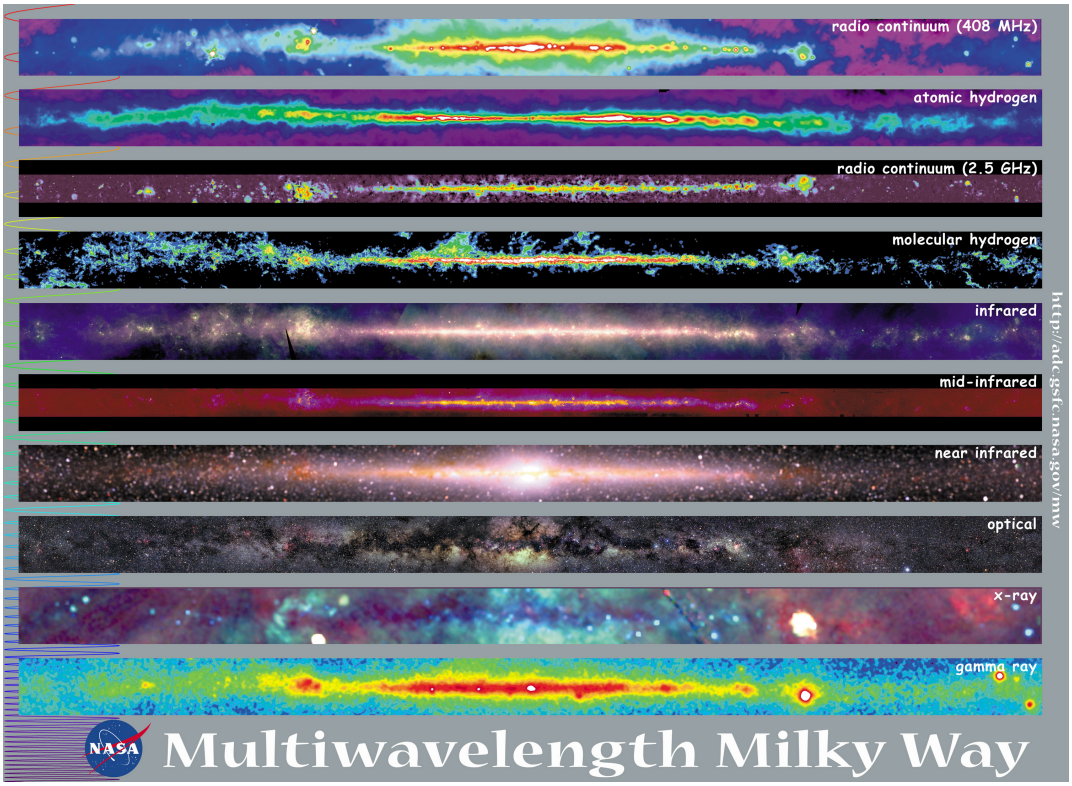

Figure 1.15: Observations of the Galactic plane traced by multiple sources: radio, H I, CO, infrared, optical, X-ray, and gamma rays. Image taken from; http://mwmw.gsfc.nasa.gov/mmw_product.html.

1.4 The Interstellar Medium

Aside from stars, galactic discs are composed primarily of the inter-stellar medium (ISM), a mix of material, primarily consisting of gas and dust. Simply by looking through the plane of our Galaxy (Fig. 1.1) or the disc of M51 (Fig. 1.4) shows dark absorbing material, the ISM dust specifically, that appears to be blocking out the starlight. Figure 1.15 shows the disc of the Milky Way at various wavelengths, each of which corresponding to a different galactic source; including several ISM species. Of specific interest are the second, third, fourth and fifth panels showing emission from H I, H II, H_2 (i.e. CO) and dust. In general the ISM is extremely tenuous, with densities approximately twenty orders of magnitude lower than the Earth's atmosphere.

Various chemical and cooling processes in the ISM that are relevant to the work in this thesis will be discussed in detail in Section 2.3, while here we only give a short overview. Many molecular species are present in the ISM, including but certainly not limited to, H_2, CO, CH, CN, CS, OH, HCN, NH_3 and H_2CO, with some tracing slightly different ISM populations (De Becker 2013). For the purposes of the work in this thesis, we are interested in CO and H_2.

H I

Atomic hydrogen, H I, is the simplest and most abundant element in the known universe and is the dominant component of the ISM. It is commonplace in disc galaxies and scarce in ellipticals, with total mass fractions ranging from 1-30% (elliptical-disc-irregular, Balkowski 1973). The primary electronic transition is the Lyman α line, seen in the UV, which can be used to map local galactic emission (Jenkins & Savage 1974; Shull & van Steenberg 1985), but at larger distances increased dust extinction makes observing this transition impossible.

A clear feature in the radio owing to the 21-cm spin-flip hyperfine transition[7] makes observing atomic gas throughout a galactic disc possible and was independently first detected by Ewen & Purcell (1951) and Muller & Oort (1951). This transition is one of the most important tools for ISM and galactic scale observations as it allows for the tracing of the interstellar gas component with minimal effects of dust extinction. The temperature required for the transition is much below that of the ISM. While the Einstein-A coefficient is very low (indicating a very long lifetime) the H I is so abundant that the transition line is easily detected. The H I traces spiral features strongly in external galaxies in the outer disc, though it tends to be scarcer in the galactic centres (e.g. M31; Chemin et al. 2009 and M81; Rots & Shane 1975). Atomic H I can be used to trace spiral features in our Galaxy(Nakanishi & Sofue 2003; Levine et al. 2006), though exact distance determinations of arms from H I are subject to some uncertainty (Burton 1973). The 21-cm line is seen in both emission, absorption (seen as gaps in the radio continuum), and self-absorption (shows cold H I absorbing 21-cm emission from warmer H I component).

Results from various surveys of Galactic H I will be discussed later in this chapter, the chemical network relevant to this work is discussed in Chapter 2 and the specifics behind simulation of the 21-cm emission line in Chapter 4.

H II

Singularly ionised hydrogen (H II) is also observed in galactic discs, and has been primarily ionised by the most massive and luminous of stars of O or B classification. H II is also seen in planetary nebulae and supernovae remnants. The H II is observed in the UV, visible and IR stemming from collisional excitation and recombination effects. H II can be observed in the optical, mostly by the Balmer lines (Hα, Hβ and Hγ) seen as hot ionised gas in the process of stabilising an electron to a ground state. These are seen in spiral galaxies as bright, condensed features within spiral arms and are believed to trace sites of star formation (see the red globules along the arms of M51 in Fig. 1.4). They are especially useful in mapping out our own Galactic structure due to their discrete nature and association with arms (Georgelin & Georgelin 1976; Russeil 2003; Hou et al. 2009).

[7]Hyperfine structure splitting stems from the split in the F quantum number, where $F = J + I$. J is the electronic angular momentum, $J = L + S$ and I is the nuclear spin which is 1/2 for H I. For the lowest energy state of H I we have one p^+ ($I = +1/2$), and an e^- in the ground state ($n = 1$). As such $L = 0$ ($L \leq n - 1$) so $J = \pm 1/2$ as $S = \pm 1/2$ for e^-'s. H I can either have $F = 1$ for e^- and p^+ parallel spins ($I = J = S = +1/2$) or $F = 0$ for antiparallel spins ($I = +1/2$, $S = J = -1/2$). The change in e^- spin causes the $\Delta F = 1$ hyperfine split, with the upper and lower states having slightly different energies, producing the 21-cm transition with an Einstein-A co-efficient of $\approx 10^{-15}\ s^{-1}$ (Combes et al. 1995).

H_2

The most abundant molecule in the ISM is molecular hydrogen (H_2). It is in the unfortunate position of being axisymmetric and therefore having no inherent dipole moment. This means there are no molecular $\Delta J = \pm 1$ transitions. There is no fine or hyperfine structure, making it effectively invisible in the radio or IR and difficult to observe with the effects of interstellar dust extinction (Field et al. 1966). Molecular hydrogen transitions don't appear until the rotational quadrupole regime of $\Delta J = \pm 2$ in the μm region, where higher energies are required to start a transition, requiring greater surrounding temperatures (around 500K, which can possibly be seen in shocked regions, Timmermann et al. 1996). This is high for typical molecular clouds, and so molecular hydrogen transitions are hard to spot, even then they are easily hidden by atmospheric water transitions. Even the ro-vibrational levels (requiring a vibrational transition in ν_1) fail to give anything more detectable. Molecular hydrogen can be observed at certain transitions such as electronic transitions in the UV and optical (e.g. *Copernicus*, Savage et al. 1977, and *FUSE*, Rachford et al. 2002). These observations, however, do not probe very deep into the ISM due to the effects of dust extinction (see Shull & Beckwith 1982 for a review). Tracing the molecular component of the ISM thus falls to the second most abundant species, CO (see next subsection).

The question of the formation of H_2 is still not entirely solved, but the current consensus is that it relies heavily on dust grains acting as a catalyst. H I is captured by the grains (if the grains are sufficiently cold) which is then allowed to tunnel through the surface to a stable point. In this hydrogen "sink" it sits until another H I interacts with it, bonds to the H I on the grain, and then easily breaks the bond to the surface, escaping into the ISM (Gould & Salpeter 1963; Hollenbach & Salpeter 1971). This process occurs inside dark clouds, with sufficient dust to catalyse the formation, and shielding both by dust and other H_2 molecules against immediate photo-destruction (Draine & Bertoldi 1996). There are also possibilities for chemically creating molecular hydrogen in the pure gas phase (Dalgarno & McCray 1973). Most of this requires either high ion supply (as in the early universe) or high temperatures, and is much less efficient in cold clouds where H_2 is easier maintained.

The amount of molecular hydrogen is measured by the H_2 fraction, which is quantified as

$$f_{H_2} = 2N(H_2)/\left[N(\mathrm{H\,I}) + 2N(H_2)\right] \approx 2N(H_2)/N(H_{tot}) \tag{1.12}$$

ranging from 10^{-7} to near 0.8 depending on environment (Binney & Merrifield 1998). The f_{H_2} ratio is a strong function of column ISM density, where diffuse clouds with insufficient UV shielding cannot protect their molecular content from photo-destruction (Spitzer et al. 1973).

CO

The task of tracing the molecular content of the ISM then falls to the next most abundant molecule; carbon monoxide ($CO/H_2 \approx 6\times10^{-5}$, Combes et al. 1995). Due to its asymmetry, CO has a readily detectable rotational transition ($J = 1 \rightarrow 0$) at a low enough energy, 2.6mm, to be seen in fairly cold clouds at 5.5K (the $J = 2 \rightarrow 1$ transition is also visible). This makes it the best tracer of molecular regions, due to the relative clarity of the radio regime. The higher strength of this

transition compared to the 21-cm H I line compensates for the much lower abundance of CO in relation to H I (Binney & Merrifield 1998).

The CO is assumed to spatially coexist with H_2. A conversion factor, $X_{CO} = N_{H_2}/I_{CO}$ is used to infer the amount of molecular hydrogen rather than observing it directly. It is defined as (Strong et al. 1988; Scoville et al. 1987)

$$X_{\rm CO} = N_{\rm H_2}/I_{\rm CO} \approx 2 \times 10^{20}\,{\rm cm^{-2}\,K^{-1}\,km^{-1}\,s} \tag{1.13}$$

where $I_{\rm CO}$ is integrated CO brightness temperature (K km/s), and N is the column density. While the $X_{\rm CO}$ value is assumed to be constant across the Milky Way, this value is subject to some variation with metallicity and density in different galaxies (Binney & Merrifield 1998; Narayanan et al. 2012).

CO itself is formed primarily through gas-phase transitions, with other C, H and O species. The isotopologues are also useful tracers, in case the CO itself becomes too optically thick. $C^{13}O$ is especially useful for temperature determinations (12CO/13CO ≈ 60-90). In the densest regions the photon from the CO rotational transition can be re-absorbed, and so masking the transition to observations, and observers can turn to the more optically thin 13CO to trace the densest cores (Combes 1991).

The study of CO has given observers their main window on cold molecular clouds, with temperatures in the range 5-20K (Young & Scoville 1991), Molecular material in general also traces out the global spiral structure of galaxies (e.g. M51; Schinnerer et al. 2013, various external galaxies; Helfer et al. 2003, and the review of Young & Scoville 1991). CO has the added advantage of having a much higher arm-interarm contrast than H I, which is present throughout the Galactic plane (Dame et al. 1986; Grabelsky et al. 1987), allowing for the finer tracing of arm features than the atomic gas.

Dust

Dust accounts for most of the attenuation effects in disc galaxies and also plays a key role in the star and planet formation processes. The term dust encompasses solid phase material that ranges in size from a few molecules to substances up to a few microns in size that cannot be considered in the atomic gas stage. This includes silicates, carbonaceous materials and polycyclic aromatic hydrocarbons[8] (PAHs) (Draine 2003). This dust acts to absorb and scatter away starlight, blocking out much of our own Galaxy from optical observations (see Fig. 1.1). As can be seen from Figure 1.15, dark dust bands appear in the optical and X-ray, but diminish in effectiveness as wavelengths move further into the infrared, and to greater wavelengths. The extinction (the collective term for dust scattering and absorption) caused by this dust is referred to as “redenning”, due to the dust primarily absorbing in the blue end of the optical spectrum, the strong effect of which was not truly appreciated until the work of Trumpler (1930). The effects of dust on molecular ISM chemistry will be discussed in Section 2.3.

[8]PAH’s are simply a hydrocarbons composed of carbon rings with outer hydrogen atoms. See Tielens (2008) for a review.

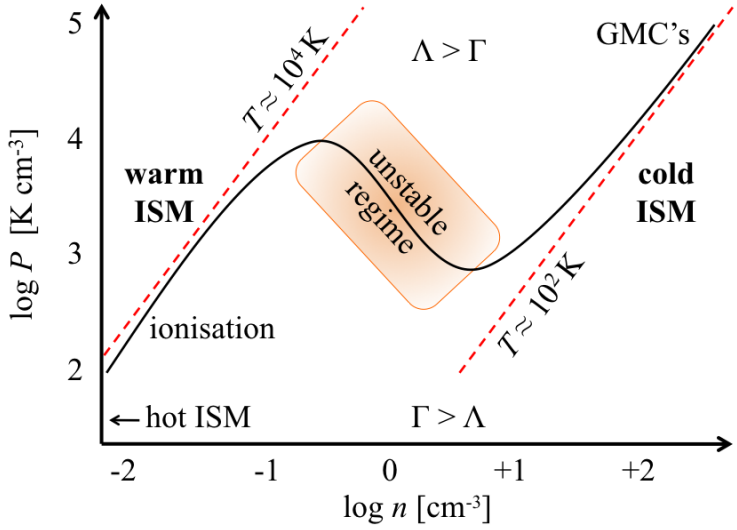

Figure 1.16: ISM phase diagram of pressure and density, based on the work of Field et al. (1969). Stable warm and cold ISM components exit with temperatures of the order 10000K and 100K respectively, joined by an unstable regime where runaway cooling/heating will return the gas to a stable regime. The various other phases, such as a very cold molecular phase and hot ionised phase, are not included in this diagram.

1.4.1 Phases of the ISM

The ISM is a very complex place, with numerous different astrophysical, radiative, and chemical processes continuously changing its thermodynamical properties. The processes relevant to the ISM gas on a galactic scale will be discussed in detail in Section 2.3. These include photoelectric heating on dust grains, cosmic ray heating, fine structure cooling, collisional ionisation, recombination cooling and molecular cooling. When all these cooling and heating effects are incorporated, a phase diagram can be produced of the ISM, similar to that shown in Figure 1.16, based on diagrams of Field et al. (1969); Wolfire et al. (1995); Liszt (2002); Cox (2005). The specifics of such a phase curve are not universal, and the exact shape is defined by the location, defining the various metallicities, abundances and fluxes that dictate the strength of individual cooling/heating rates (Wolfire et al. 1995; Liszt 2002). The diagram shows two distinct branches, indicating the two phases of the original Field et al. (1969) model; the cold neutral medium (CNM) and warm neutral medium (WNM). Each of these regions has approximately stable temperatures (of the order $<$ 100K and 10000K respectively). They are separated by an unstable region[9], with temperatures ranging from 200K to approximately 5000K (Cox 2005). In this region the gas experiences runaway cooling/heating until it joins one of the aforementioned stable branches.

This model helped explain the apparent discrepancy between observations of ISM gas with

[9]This is caused by the negative gradient in the "loss function", defined as the net heating/cooling rates; $\dot{E} = \Gamma + \Lambda$. The derivate of this function (i.e. the second derivative of the change in energy) defines the location of an unstable/stable equilibrium state. For example, $d\dot{E}/dn > 0$ signifies a stable point, while $d\dot{E}/dn < 0$ an unstable point.

Component	T [K]	n [cm^{-3}]	Notes
Molecular (MM)	10-20	10^2-10^6	Dominated by H_2 and CO, observed in radio
Cold atomic (CNM)	50-100	20-50	H I dominated, moderate density, H I absorption
Warm atomic (WNM)	6000-10000	0.2-0.5	H I dominated, diffuse, H I emission
Warm ionised (WIM)	≈ 8000	0.2-0.5	H II dominated, observed in H_α
Hot ionised (HIM)	$\approx 10^6$	$\approx 10^{-3}$	H II and ionised metals, observed in X-ray and UV

Table 1.1: Properties of the five main ISM phases believed to be present in the Galactic ISM, ordered by temperature. Adapted from Ferrière (2001).

contrasting temperatures and pressures. This two-phase model was then expanded to incorporate hot ionised media which are a result of supernovae winds heating up the surrounding ISM, creating H II "bubbles" (Cox & Smith 1974; McKee & Ostriker 1977). The warm medium was expanded to include both ionised and neutral components, with comparable densities and pressures. These multi-phase models are not without their flaws however. Models by Slavin & Cox (1993) found that the size of supernova bubbles may have been somewhat overestimated in the McKee & Ostriker (1977) multiphase model, undermining their importance in ISM thermal structure. The key assumption of local thermal pressure balance between the various phases may also be an incorrect one, and various other pressure sources such as magnetic fields and cosmic rays radiation pressure may be important (e.g. large thermal pressure variations were seen in the local ISM by Bowyer et al. 1995). Observations and simulations have also seen that the unstable regime shown in Figure 1.16 can be surprisingly well populated, despite the expected instability (e.g. Heiles & Troland 2003).

Nethertheless, the multiphase model of the ISM is still one of the better formulations of the ISM's various components (Cox 2005). The properties of the generally accepted 5-phases of the ISM are given in Table 1.1 (adapted from Ferrière 2001). The components are a cold and warm neutral medium (C/WNM), a warm ionised medium (WIM), which between them contain most of the galactic gas mass budget. The WIM traces gas that is subject to OB star UV fields. The hot ionised medium (HIM) traces the hottest gas components resulting from supernovae winds, and is found in bubbles and fountains far out of the galactic plane. Finally there is the molecular medium (MM) where the cold, dense clouds are found and are the sites of star formation.

Stars themselves have a strong influence on the ISM though various feedback mechanisms. The term feedback constitutes a variety of physical processes depending on the scale, but primarily it refers to either supernovae or stellar winds form OB stars injecting large amounts of energy into the adjacent pockets of ISM gas. The effect of feedback is to blow apart ISM gas, dissociating molecular gas in photodissociation regions (PDRs) and ionising gas in H II/HIM regions. Feedback also creates holes in the H I distribution (e.g. seen in IC 2574 by Walter & Brinks 1999 and M31 by Brinks & Bajaja 1986), and imparts thermal energy allowing for the expansion of shells into the ambient ISM. These expanding shells can eventually cool at sufficient distances from the feedback source, and can then host cold and dense gas. This could eventually host further star formation (e.g. Cioffi et al. 1988, McCray & Kafatos 1987), though winds could also act to break apart and destroy clouds and inhibit star formation (Dale et al. 2013).

1.5 Determining Galactic structure

Despite the difficulty in doing so, studies of the global structure of the Milky Way have been numerous in the past five decades. Due to the position of the Earth within the Galaxy many techniques have been used to try and circumvent the problem of discerning the shape of the body whilst inside it. In this section we briefly outline some of the main techniques used in the literature for determining galactic structure. Key findings based on these methods will be discussed in the next section.

1.5.1 Methods of structure determination

Method 1: Determine actual or kinematic distances

The most obvious method of determining Galactic structure is to simply measure the distance to sources in the Galaxy across various Galactic longitudes. For example through stellar parallaxes (distance and magnitude limited), trigonometric parallaxes (if close enough to the Earth), OB star standard candles, main sequence fitting, or through Cepheid variables. The problem is that many of these cannot be assumed to be tracing spiral structure, simply just the global disc-like structure of the Milky Way. The objects this is actually possible for is minimal and distances are only accurate to approximately 10%, making the larger distances more uncertain (Elmegreen 1985). Nevertheless, some spirality can clearly be seen in these measurements (Becker & Fenkart 1971; Vogt & Moffat 1975).

The more widely applicable method of determining distances is to use the velocity information of the source to calculate a kinematic distance. By using the velocities from emission lines of ISM gas complexes such as H I and CO a distance can be calculated so long as some velocity field of the Galaxy is known, which can be calculated from the rotation curve. The line-of-sight velocity, v_{los}, measured from the emission profile as a function of galactic longitude, l is

$$v_{los}(l) = R_\circ \sin(l) \left[\Omega(R) - \Omega_\circ\right], \tag{1.14}$$

where the gas is located at a radius R from the galactic centre (Shu 1982) and $\Omega_\circ$ is the angular velocity at the Solar position. If we simply substitute for the rotation frequency $\Omega(r) = V(R)/R$ we can re-arrange to give the Galactocentric radius of the emitting gas,

$$R = R_\circ \sin(l) \frac{V(R)}{v_{los} + V_\circ \sin l} \tag{1.15}$$

where v_{los} can be directly obtained from the emission profile, l, $R_\circ$ and $V_\circ$ are known (the position and velocity of the Earth's position) and $V(R)$ can be either taken from the known rotation curve or directly evaluated from emission profiles[10]. Fortunately the Galactic rotation curve is fairly well

[10]First evaluate Equation 1.14 for the smallest radius possible along the line of sight which is equivalent to $r_{\min} = R_\circ \sin l$. Then Equation 1.14 becomes $v_{los}^{\min}(l) = r_{\min}\Omega(r_{\min}) - V_\circ \sin(l)$ giving $V(r_{\min}) = v_{los}^{\min}(l) + V_\circ \sin(l)$. This gives a $v - r$ pair for the rotation curve, providing you can obtain the maxiumum line of sight velocity (corresponding to minimum radius) from the emission profile. This is done simply by observing where the emission sharply drops off at velocity extrema (Binney & Merrifield 1998).

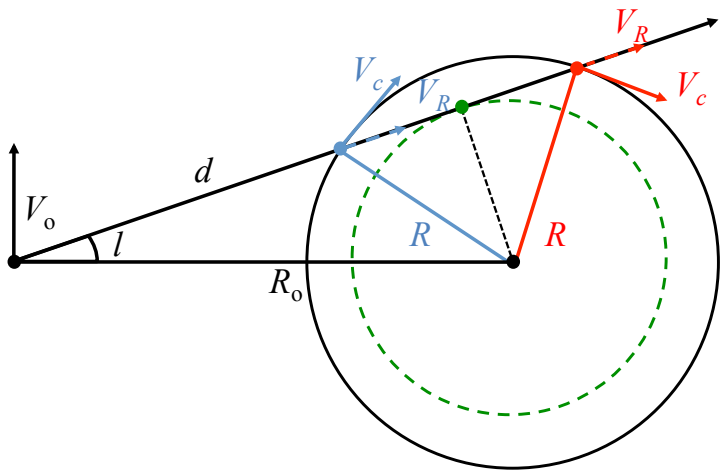

Figure 1.17: Kinematic distance problem in our Galaxy when observing gas with a radial velocity of V_r and circular velocity of V_c at some distance R from the Galactic centre. At any point a single radius and radial velocity corresponds to two separate distances from the Earth (red and blue lines intersection with the d line). Based on Figure 1 of Roman-Duval et al. (2009).

measured, and is approximately axisymmetric (Brand & Blitz 1993). While this method works well for calculating distances outside of the Solar circle, there is a degeneracy in distance when looking inside. Figure 1.17 illustrates this "distance ambiguity". There are two points that have the correct observed line-of-sight velocity calculated from the emission profile, one at a near (blue line, Fig. 1.17) and one near distance (red line) compared to the the smallest possible Galactic radius (dashed line) and point of maximum velocity observed from the profile. By simply calculating the distance, d, to the emitting gas shown in Fig. 1.17 you see that there are two distinct solutions;

$$d = R_\circ \cos(l) \pm \sqrt{R^2 - R_\circ^2 \sin^2(l)} \tag{1.16}$$

where d is the distance from the observer to the point of maximum velocity.

There have been numerous different techniques developed to break this degeneracy. Observations of H II regions by Downes et al. (1980) also measured OH or H_2CO absorption lines towards the same direction as the sources. If the shift in these lines implied a velocity much larger than the H II region they assumed the emission is from different sources and the emission from the H II travelled from the larger kinematic distance through OH/H_2CO. If the difference in velocities is small it is still somewhat ambiguous, due to streaming velocities and random dispersions possibly causing the small offset (Elmegreen 1985). Kolpak et al. (2003) use this method by using additional observations of H I in their H II survey to map out the Galaxy inwards of the Solar circle and Roman-Duval et al. (2009) use H I self-absorption (HISA) to eliminate the ambiguity in their CO survey, where additional HISA would be seen for the far-kinematic distance as opposed to the near distance. This method is widely employed for a number of different tracers (Araya et al. 2002; Russeil 2003; Sewilo et al. 2004; Watson et al. 2003; Fish et al. 2003; Paladini et al. 2004; Pandian et al. 2008). Another method requires the construction of theoretical density maps of the Milky Way, that are then used to estimate the column density viewed from Earth, from which we

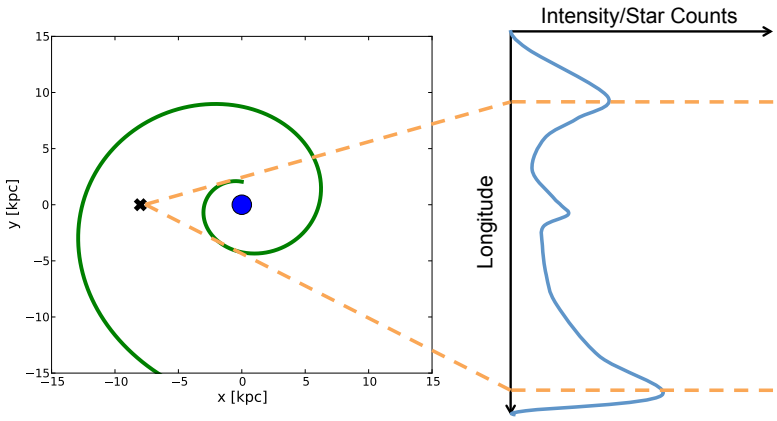

Figure 1.18: Tangency method for determining spiral structure. On the left is the top-down structure with the observer at the black cross in a galaxy with a one-armed spiral over-density. On the right is the star count/emission profile as a function of longitude, with over-densities caused by the spiral arm tangents appearing as peaks in the distribution. This is a simplified case, and in reality an exponential disc profile is seen superimposed in the observed profile.

can infer what distance the material lies (Nakanishi & Sofue 2003, 2006; Levine et al. 2006).

The main source of error is the uncertainty in the rotation curve, local velocity dispersion in the gas, or steaming at velocities significantly different to those implied by the global rotation, and is of the order 10-20% (Elmegreen 1985). The relatively large uncertainties and numerous different approaches that exist in the literature for solving the distance ambiguity make structure determinations from kinematic distances open to interpretation.

Somewhat troublingly; kinematic and direct distance determinations can yield different results, highlighting uncertainties in any distance determinations. For instance, Moisés et al. (2011) found that for a selection of H II regions trigonometric distances tended to be smaller than the kinematic distances. Using a simulated Galactic disc Gómez (2006) showed that kinematic distances return a distorted and spurious Galactic structure. While they also showed that a better reproduction could be made using the full Galactic velocity field, this is much more difficult to obtain than a simple axisymmetric rotation curve. The rotation models used to determine these distances fail to take into account large scale shocks and the effect of spiral/barred structure on the velocity field, which can result in large departures from an axisymmetric model.

Method 2: Tangencies

A non-kinematic method for determining Galactic structure is to use star counts or emission strength as a function of longtiude. In cases where stellar distances are not known the non-symmetric nature of the stellar distribution or dust emission with longitude can show over dense regions that can correspond to spiral/bar features. These spikes in the galactic emission profile stem from spiral arm tangencies seen from Earth and result from an increased density when looking down a long, continuous stretch of arm. By identifying the same arm in two separate quadrants we can also directly compute the pitch angle (Drimmel 2000). Another advantage of these kind of

observations is that by matching the global shape of the emission/star counts we can reverse engineer a surface density of the galactic disc, bulge and bar. These models can be then used directly in numerical simulations to set up the galactic stellar distribution (Benjamin 2008).

This method is illustrated in Figure 1.18. To the left is a top-down view of a simple one-armed spiral galaxy, where the observer is placed at the black cross. To the right is the emission/star count profile as a function of longitude in the inner galaxy. Peaks exist in the distribution when looking along an arm tangency, i.e. when orientated down a sight line that spans the longest stretch of spiral arm. A peak is also shown for the Galactic centre. This method is obviously only suitable for observations in the inner disc, and in reality the profile of the entire stellar disc will also be seen, as a steady decay in counts/emission as we look away from the Galactic centre. Bars are expected to appear as asymmetries around the Galactic centre, provided that the bar is angled far from the perpendicular to the line-of-sight to the Galactic centre.

Method 3: Longitude-velocity maps

A method of determining Galactic structure that is free from model assumptions, yet still allows for the tracing of spiral arms is to map out the position of sources in velocity space. An example of one of these longitude-velocity, *l*-*v* , diagrams is shown in Figure 1.19. In the left panel a simple disc galaxy is shown, with the observer placed at the black cross within some disc of material (grey circle). Two spiral arms have been included for illustration of the method (red and green lines). In the right panel is the corresponding *l*-*v* map, constructed using the same rotation model as that of the right panel of Fig. 1.7. The over-densities at the spiral arms will appear against the continuum of the disc, from which pitch angles can be directly measured. Spiral arm tangencies should also be seen as bright concentrations near peak velocities with longitude (if measuring emission). The terminal velocity curve can also be used to determine the rotation curve of the inner Galaxy independently for the first and fourth quadrants, assuming $R_\circ$ and $V_\circ$ are known (Binney & Merrifield 1998). Rings, bars, arms, expanding features, and non-circular motions will all impact the *l*-*v* plot, making the determination of the exact morphology of the underlying feature somewhat ambiguous.

This method has been used with a variety of different tracers including H I (Burton & Shane 1970; Weaver 1970; Henderson 1977; Hartmann & Burton 1997; Kalberla et al. 2005), CO (Cohen et al. 1980; Solomon et al. 1985; Dame et al. 1986; Grabelsky et al. 1987; Dame et al. 1987, 2001), H II (Lockman 1979; Downes et al. 1980) and $C^{13}O$ (Stark & Lee 2006; Bally et al. 1987). One of the main advantages of using gas emission is that the intensity as a function of *l*-*v* can provide additional information, as opposed to say the position of discrete sources such as H II regions in *l*-*v* space. The structure of emission as a function of latitude can also provide information on the scale of specific structures, highlighting features that may otherwise be missed in an integrated map (e.g. Dame & Thaddeus 2011). Full surveys of the Galactic plane require large amounts of observing time, so it is more common to find studies concentrating on certain regions, such as the Galactic centre. A top-down map can be constructed from these *l*-*v* observations but will again require a Galactic rotation model .

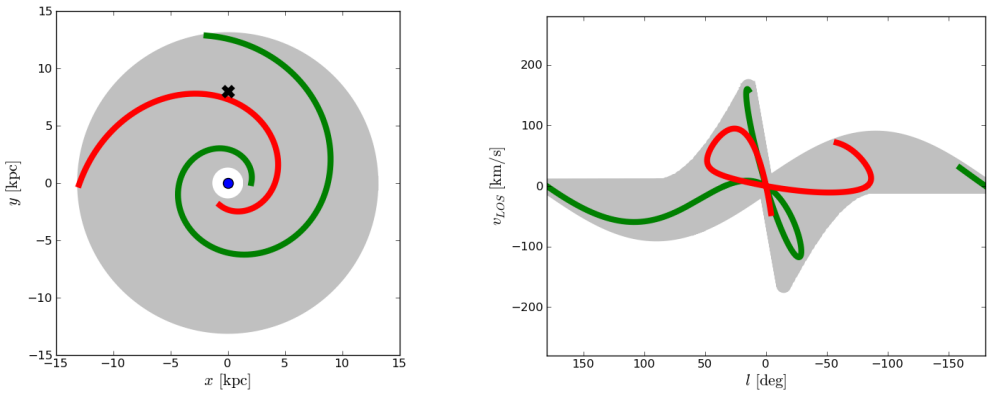

Figure 1.19: Projection of a Milky Way like disc and spiral arms from $x - y$ (left) onto $l - v$ (right) space using the rotation curve of the right panel of Fig. 1.7. The spiral arms appear as over-densities in $l - v$ space on the backdrop of the axisymmetric disc (shown in grey). Two spiral arms are shown, the arm in green has $\alpha = 13°$ and the red arm has $\alpha = 20°$, both are logarithmic in shape. The observer is placed at the black cross in the left panel with $l = 0°$ directed towards the Galactic centre.

As some of the results from the above methods are open to interpretation, numerical simulations are often used to attempt to reproduce the observations. If a model can be made that sufficiently reproduces the observations then the Galactic morphology underlying the model is a good representation of the Galaxy. This is in essence the approach adopted in this thesis, and will be discussed in detail later in this chapter.

1.6 Observational studies of Milky Way morphology

Many investigations into the structure of the Milky Way have been under-taken in the past half-century. While a combination of observational and computational studies have made progress by constraining arm and barred structure there is still no clear consensus on the Galactic morphology. The current best-guess is that the Milky Way is a four-armed spiral with a pitch angle of $10° - 20°$. The wide range of pitch angle depends on Galactic radius, with wider pitch angles inferred from the outer disc (e.g. Levine et al. 2006). There is however some support for a two-armed model, in which case the pitch angle is better fit by a much lower value. There is believed to be at least one inner bar, and some studies suggest a second with a different morphology and orientation. Finally some suggest a ring of molecular material may exist around $R = 5$kpc, though observational evidence could be due to an arm instead (e.g. Dobbs & Burkert 2012). In this section we will recount some of the major and more convincing evidence for these morphological features. For a more in depth take on all the studies in the literature the reader is directed to the works of Elmegreen (1985), Vallée (1995, 2002, 2005, 2008), Efremov (2011) and the proceedings of Benjamin (2008).

1.6.1 Structure: top-down reconstructions

Early investigations focusing on the distribution of hydrogen seemed to disagree from the outset. Weaver (1970) favoured a 2-armed, 12.5°structure in their analysis of H I, though this requires the existence of numerous spurs minor interarm features. However, the Parkes H I survey suggests a much tighter multi-armed structure (Kerr 1969a,b), with the singular agreement between these two studies being the positions of spiral tangents (Simonson 1970). The seminal ionised hydrogen maps of Georgelin & Georgelin (1976) (hereafter GG76) also favour a 4-armed spiral fit (of 12°), though largely based on kinematic distances. This model became the standard for the Galactic spiral map for some time, owing to the strong correlation of H II features with a spiral model (as opposed to H I maps at the time that often have a large amount of off-arm material). A variant of this model is shown in the left panel of Figure 1.20, showing the kink in the arms near the Solar position. Some studies even suggested a middle ground solution, such as the analysis of existing H I data in *l*-*v* space by Simonson (1976) who favoured a 2-armed 6-8° inner spiral branching into a 4-armed 16° spiral outside of the Solar circle.

The study of Caswell & Haynes (1987) finds that H II regions measured within $l = 0 - 180°$ are a reasonable match to the 4-armed model of GG76. Dame et al. (1986) find that measured CO cloud complexes within the first quadrant fit a multi-armed spiral structure with pitch angles between 5-12°. In another study of molecular clouds by Grabelsky et al. (1988) in the inner Galaxy, the authors determine that CO features are well matched by a single 10° logarithmic spiral, though their range of longitudes is somewhat limited. Worthy of note are the several studies that are not focused on various ISM gases. For instance, the works of Vallee (1988), Simard-Normandin & Kronberg (1980) and Han & Qiao (1994) use pulsar and extragalactic rotation measures[11] (RM) to discern the shape of the Galaxy's magnetic field. They tentatively show that the magnetic field is directed in a logarithmic spiral pattern, rather than a series of concentric rings, with Han et al. (1999) and Indrani & Deshpande (1999) specifically favouring a 4-armed spiral configuration. In a similar vein, Taylor & Cordes (1993) (hereafter TC93) construct a map of free electrons using the model of GG76, and show that using this they can obtain pulsar *dispersion measures* leading to pulsar distance measurements that are a very good match to actual measured distances, which in turn give further credibility to the 4-armed model. The spiral arm model adopted in their work superceedes that of GG76 as the literature standard for comparisons in other works, and is shown in the left of Figure 1.20 (see also Cordes & Lazio 2002 and Drimmel et al. 2003). An important point to note is that many studies of morphology are heavily influenced by the existing literature, for instance the TC93 model is a refinement of the GG76 model. In many cases studies will simply show a distribution is good by-eye match for the "standard" 4-armed case, with little consideration given to other possibilities. Amaral & Lepine (1997) use the positions of nearby open clusters to try and discern between a 2 and 4 arm structure. They find that a 2-armed (inner) superimposed on a 4-armed (outer) structure of 14°can match the positions and bridge the 2/4-armed discrepancies. Their modelling is only confined to the Solar neighbourhood however, and many clusters lie in the

[11] Rotation measures are a a radio astronomical tool for measuring the strength of magnetic fields. When light passes through a region with a non-negligible magnetic field the light becomes polarised. The effect of the light polarisation is proportional to the strength of the field along the line-of-sight, and the number density of free electrons: $\mathrm{RM} \propto \int n_e \vec{B} \cdot \mathrm{d}\vec{s}$.

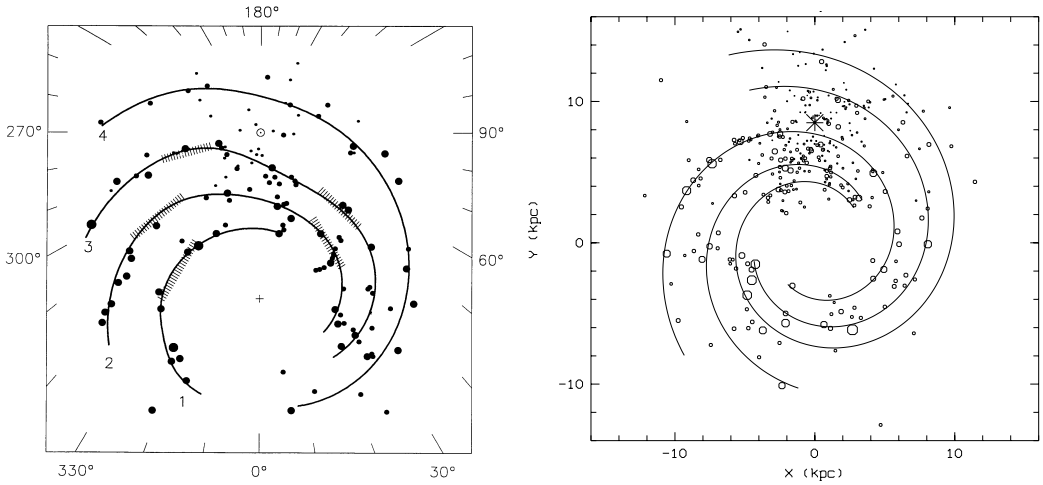

Figure 1.20: Two studies of distance determinations in the Galaxy. Left: H II regions mapped by Taylor & Cordes (1993) shown with a variant of the arm model of Georgelin & Georgelin (1976). Tangencies are shown as hatched regions. Right: star forming complexes (H II, CO, OB stars) mapped by Russeil (2003) with their best-fitting logarithmic spiral model.

interams of their best fit.

The works of Kolpak et al. (2003), Fish et al. (2003), Sewilo et al. (2004) Watson et al. (2003) and Paladini et al. (2004) measured the distances to several H II regions. The distance measurements of the three latter studies agree reasonably well with the 4 spiral arms of TC93. Yang et al. (2002) measure distances to a large number of CO sources, many of which correlate well with the nearby Sagittarius arm. Despite their large number of sources, few can be attributed to any other arm features, and their sample selection is biased against targets less than 5 kpc from the Galactic centre. The spatial distribution of high and low mass X-ray binaries studied by Grimm et al. (2002) shows while low mass binaries show no real preference towards any spiral pattern, the high mass binaries trace a 4-armed spiral pattern (be it that of TC93 or a simple symmetric 4-armed, 12°spiral).

Nakanishi & Sofue (2006) measure the H I distribution (in column density) throughout the galactic disc. They find that the distribution is in fact best described by a 3-armed logarithmic spiral, with pitch angles ranging from 7-18°. They find no evidence for the existence of the Scutum-Crux arm, or any strong H I emission 5 kpc from the Galactic centre. Using numerous H II complexes, Russeil (2003) perform a full fit to spiral arm parameters, and their data is shown in the right of Figure 1.20 with their best fitting model. A spiral pattern is clearly visible by-eye, and they find that a 2-armed model is insufficient to fit their complex distances. Their data seems to fit a 3 and 4-armed spiral reasonably well, with pitch angles around 11°. The main difference between their 3 and 4-armed fits is whether the Norma arm joins to the Cygnus or Perseus arm (see Fig.1.24). An important aside when viewing Figure 1.20 is that the spiral pattern is becoming less clear the more recent the study, and the more detail that becomes available. Specifically the distribution of sources < 3kpc from the Earth displays no clear structure, which explains the uncertainty in the Carina arm as $l \rightarrow 0°$ and the nature of the Local arm.

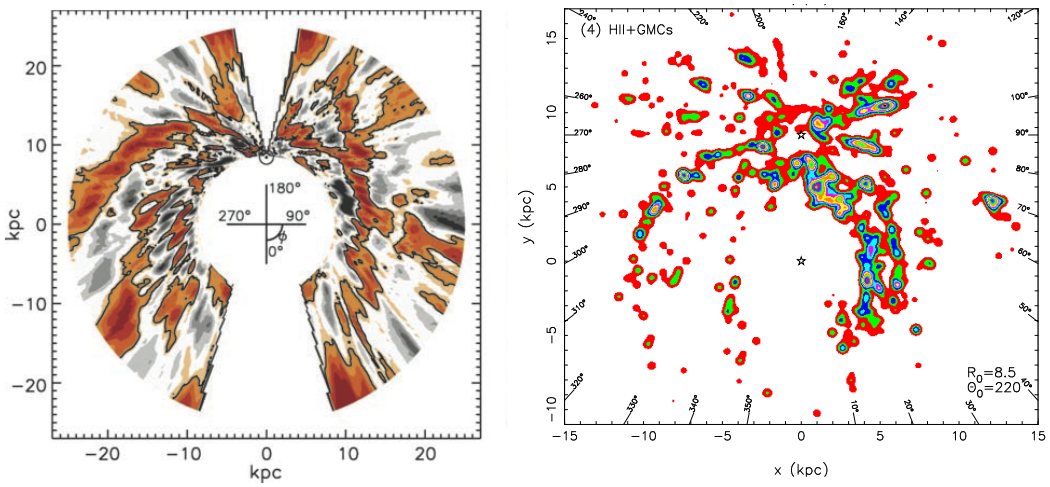

Figure 1.21: Two studies of Galactic kinematic distance determinations. Left: H I normalised surface density in the outer Galactic disc from Levine et al. (2006). Right: H II region and GMC distribution from Hou et al. (2009).

Levine et al. (2006) fit an asymmetric 4-armed spiral with $\alpha \approx 23°$ in their analysis of H I in the outer ($6 < R < 40$ kpc) Milky Way. A symmetric spiral model is investigated, but the H I in the fourth quadrant requires three arms of small separation. Their map is reproduced in the left of Fig. 1.21. The authors note the pitch angles are rather large compared to previous studies, and that this may indicate the arms are unwinding in the outer disc. Larger pitch angles in the outer galaxy compared to the inner galaxy have been suggested in previous studies (e.g. Simonson 1976). In more recent work by Hou et al. (2009) the authors fit different spiral arm models to H II and GMC literature data (right, Fig. 1.21). They find best-fitting values for α of approximately 5, 8, and 10° for 2, 3 and 4 armed models respectively, finding that the 2-armed model is a much poorer fit to the data. The distribution of CS mapped by Lépine et al. (2011) also provides a strong indication of spiral structure. They attempt to fit the actual orbital resonances that drive density waves, and fit a 4:1 box-like resonance to the inner 7kpc, which can produce a 4-armed spiral structure.

1.6.2 Structure: tangency profiles

Some of the most conclusive evidence of spiral structure comes from longitude maps with the use of the *COBE* and *Spitzer* satellites. Drimmel (2000) uses data from the DIRBE instrument aboard *COBE* to construct K-band and 240μm (dust) emission profiles for $|l| \leq 90°$, shown in the left of Figure 1.22 left (K: top, 240μm: bottom). The central peak is from the galactic bulge/bar and the global emission profile drops off in accordance to the Milky Ways exponential disc. The K-band emission shows weaker structure compared to dust emission but what structure is there is mirrored between the two. The authors indicate 5 prominent features labelled S_1, C_1, T, S_2 and C_2, with the S tangent points belonging to the Scutum-Crux arm, C belonging to the Sagittarius-Carina arm and the T point to the 3-kpc arm. The minor Orion arm can be seen at $l = 80°$ in the emission but it's strength is over-exaggerated due to it's close proximity. The K-band and 240μm emission have distinct differences. The most striking being the lack of any conclusive tangency features

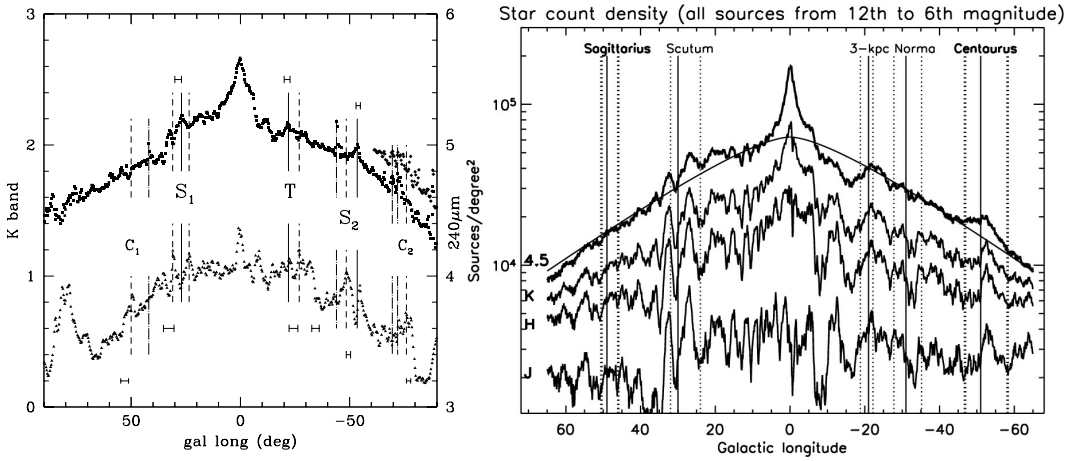

Figure 1.22: Two examples of Galactic arm tangency profiles. Left: *COBE*/DIRBE emission from old stellar population (K-band, top) and dust (240μm, bottom) from Drimmel (2000). Right: *Spitzer*/GLIMPSE source counts in the J, H, K and 4.5μm bands from Churchwell et al. (2009). Arm tangencies are indicated by vertical lines.

at 50° or −35° in K-band compared to 240μm. They infer from this that there exists only a two armed structure in the stars (seen in the K-band emission) joining with the bar. The gas/dust then forms a four-armed pattern in response to the two armed stellar potential. This interpretation has been suggested by numerous observations (e.g Drimmel & Spergel 2001; Benjamin 2008) and has been seen in hydrodynamical simulations (e.g. Englmaier & Gerhard 1999; Fux 1999; Martos et al. 2004). This also goes some way to explain the large ensemble of different arm combinations found in the literature; there could be two or four armed perturbations depending on the observation. A later study using *COBE*/DIRBE data by the same authors find similar conclusions (Drimmel & Spergel 2001). Their best fits to the emission in dust is a four-armed spiral, while the stars (K-J band) best suits a two armed fit.

The *Spitzer* GLIMPSE Legacy program is analysed by Benjamin et al. (2005) where the authors present similar maps to Fig. 1.18 of IR sources within $10° < l < 65°$ and $295° < l < 350°$ at 4.5μm. There are tentative signs of the Centaurus and Scutum arms but no sign of other arm tangencies. The real find however is signs of the galactic bar in their source counts. There is a strong asymmetry in counts around the Galactic centre, with 25% more stars in the first quadrant compared to the fourth inside of $l < 30°$ (Churchwell et al. 2009). This agrees with the general consensus that the Milky Way's bar is orientated between $15° - 30°$ which would show up in the count maps around $0 < l < 45°$ (Gerhard 2002). They then fit to the bar's orientation and length, finding a value of 44° and a length of around 4.5kpc. Churchwell et al. (2009) also use the GLIMPSE survey to highlight spiral arm tangents in 4.5μm, K, J and H bands (shown in the right of Figure 1.22). The Scutum, 3kpc, and Centaurus arm tangents can be seen clearly in all bands but there is no clear sign of the expected Sagittarius tangency.

Steiman-Cameron et al. (2010) analyse the C II (158 μm) and N II (205 μm) lines from the FIRAS instrument onboard *COBE*, which are known to trace spiral structure to greater densities and pressures. They find strong tangent signatures of the Scutum, 3kpc, Centaurus, Carina, Sagit-

tarius and Orion arm features. By fitting logarithmic spiral models they find a four-arm pattern fits the data well. As N II and C II should trace gaseous and young stellar/star forming regions they conclude that the Milky Way is four armed in the gas, and agree with Drimmel (2000) and Churchwell et al. (2009) that the older, evolved, stellar population (i.e. K and M stars) exist in a two armed pattern. This is supported by evidence that over the many arm models over the past decades almost all tracers of young stellar populations and gas are best fit with four armed models (e.g. H II, CO, OB stars, molecular clouds, Cephids, C II and N II). On the contrary the majority of two armed models from the literature stem from observations of the older stellar population, i.e. K and M stars (Steiman-Cameron et al. 2010).

1.6.3 Structure: longitude-velocity maps

There have been numerous *l*-*v* maps constructed in the literature, predominantly using CO and H I emission (e.g. Dame et al. 1987; Hartmann & Burton 1997; Strasser et al. 2007; McClure-Griffiths et al. 2012). Two modern maps of ISM emission over the entire Galactic plane are shown in Figure 1.23. These are the H I 21-cm emission from Kalberla et al. (2005) and the CO $J = 0 \rightarrow 1$ emission from Dame et al. (2001). While higher resolution data is available for both tracers, these are the most up-to-date maps available of the *entire* plane. Spiral arm features can clearly be seen in each map, with the Perseus, Outer and Carina arms being the clearest. The Sagittarius and Local arms are less clear, the former due to the mixing with the large amount of emission towards the Galactic centre, and the latter due to the ambiguous nature of local structure ($v_{los} \approx 0\,\mathrm{km\,s^{-1}}$). There are some key differences between the two. The CO is much patchier than the H I, while the H I appears less confined to spiral arms and extends much further radially than CO. The CO displays a strong inner feature, dubbed the central molecular zone (CMZ). Asymmetric in nature, it is believed to be product of the ILR of the bar (Lee et al. 1999; Rodriguez-Fernandez & Combes 2008). There is a strong feature approximately diagonal in the CO emission in Fig. 1.23 in the inner Galaxy, that is not as distinct in the atomic emission. This has been attributed to a molecular ring of material around 4kpc in radius (Marshall et al. 2009). While rings are not uncommon in external galaxies, no substantial evidence exists that shows the feature can be better fit by a combination of arms rather than a ring (Dobbs & Burkert 2012). We will refer to this feature as the Inner Ridge of emission, as to not imply its structure as a ring or arm.

One of the more difficult tasks when determining the spiral structure of our Galaxy is detecting spiral arms beyond the Galactic centre, due to the large amounts intervening ISM dust and the strong emission towards the galactic bulge. Dame & Thaddeus (2011) find a Galactic arm beyond the galactic bulge in CO and H I *l*-*v* maps, its existence unnoticed due to it's location 3°above the galactic plane. They suggest that this new arm is an extension of the Scutum-Centaurus arm beyond the Galactic centre, an analogue to the Perseus arm, which the authors suggest supports the 2-armed picture proposed by Drimmel (2000) and Churchwell et al. (2009). Similar earlier work by the same authors (Dame & Thaddeus 2008) discovered a far counterpart to the nearby 3kpc arm in CO *l*-*v* data, further supporting a symmetric Milky Way model.

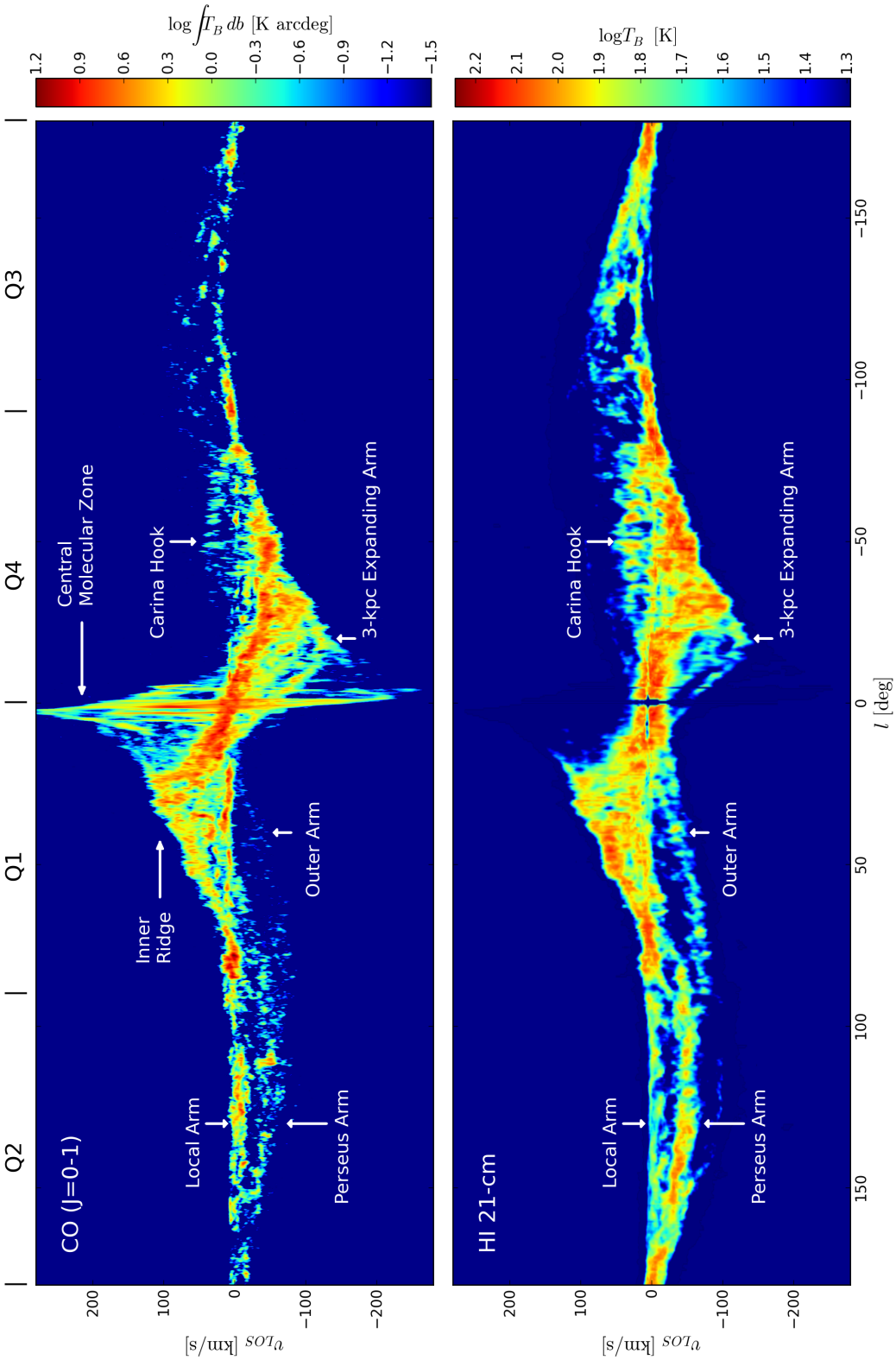

Figure 1.23: Brightness temperature emission maps of the Galactic plane in CO ($J = 0 \rightarrow 1$ transition, top) and H I (21-cm transition, bottom). H I data taken from Kalberla et al. (2005) and CO from Dame et al. (2001). Also labelled are a selection of morphological features. Due to the significantly weaker emission of the CO line, we have integrated through $b \pm 2°$.

1.6.4 Structure: the bar(s)

Specifically regarding the bar, evidence of its morphology is perhaps even less convergent than the arms. The bar appears either short and spheroidal or long and thin. The former bar is the classical bar, in that evidence for which has existed for many decades. This bar is angled at roughly 20° to the Sun-Galactic centre line and is approximately 3kpc long. This bar is commonly referred to as the *COBE*/DIRBE bar due to the most convincing evidence coming from *COBE* source counts (Blitz & Spergel 1991; Dwek et al. 1995). It is also believed to be the cause of asymmetries seen in the velocity distribution of ISM gas. The bar is also referred to as the triaxial bulge or the boxy/bulgey/peanut bar due to the shape of the best fitting mass models. See Blitz & Spergel (1991); Weiland et al. (1994); Binney et al. (1997) and the review by Gerhard (2002) for more information.

The other, "Long", bar was originally proposed by Hammersley et al. (2000) and additional evidence for which was seen in GLIMPSE data (Benjamin et al. 2005; Churchwell et al. 2009). This bar is believed to be longer ($\approx$ 4kpc) and thinner than the DIRBE bar, and much less vertically extended. The GLIMPSE data suggests the bar is angled at approximately 45°, though studies are still in their infancy in discerning whether these bars are indeed separate entities (the orientations agree within errors reported by respective studies). Regardless of which shape the bar takes, it is still unclear whether the arms join exactly to the ends of the bar, or whether there is some contact region, perhaps indicated by a ring (both cases are seen in external galaxies). There is evidence, however, that the bar does drive some spiral structures in the disc. The near 3kpc expanding arm, so named for the velocities that significantly deviate from circular rotation, has been reproduced by Englmaier & Gerhard (1999) by the inclusion of a bar, where the arm is seen to directly trail from the bar end.

1.6.5 Pattern speeds

As with external Galaxies, determining the arm and bar pattern speeds (Ω_{sp} and Ω_b) of the Milky Way is somewhat more difficult than determining the structure due to observations only probing a very small time window with respect to Galactic rotation periods. Determining the pattern speed also usually relies on some assumed morphology. For example, if the method uses the location of resonances to determine the pattern speed, these are dependant on the arm number adopted. The rotation speed of the arms is of specific interest for its creation of a co-rotation radius. Many models place the Solar position at the CR, which could in theory be a site for steady star formation due to material co-rotating with the high densities arms found in arms, though it could lessen its importance due to the lack of shocks experienced by the traversal of gas into the arms initially. An important aside is that for many of these pattern speeds the value is coupled to the local radius and circular velocity. This in itself is subject to uncertainty, with values of the Earth's Galacto-centric distance ranging from 7.0-8.5kpc and velocity from 200-230 $\mathrm{km\,s^{-1}}$(Binney & Tremaine 1987; Reid 1993).

A common method is that of Tremaine & Weinberg (1984), where the pattern speed is calculated from integrating specific velocity components across the disc. This method is designed

for external galaxies, but can be applied to the Milky Way. By applying this method to stars in our own Galaxy, Debattista et al. (2002) find a pattern speed[12] of 60km s^{-1} kpc^{-1}. However, this is simply attributed to a non-axisymmetric feature, which while seemingly reasonable for the bar, could be from the arms themselves.

By measuring the ages of open clusters, which are assumed to have been created in spiral arms, and rotating them backwards in time it is possible that they trace out spiral arms at their birthplaces. Dias & Lépine (2005) use this method give a constant value of 25km s^{-1} kpc^{-1}, though this is only for clusters near the Solar position and has additional errors associated with the age determinations of the clusters. Another method is to model the kinematics of OB and Cepheid stars, which can be constructed to contain a spiral perturbation with numerous free parameters, including the spiral pattern speed. Applications of this method suggest the arms are rotating with a speed of 22-30km s^{-1} kpc^{-1}(Avedisova & Palous 1989; Amaral & Lepine 1997; Mishurov & Zenina 1999; Fernández et al. 2001; Lépine et al. 2001).

The bar pattern speed can be estimated by use of Equation 1.10 and measuring the bar length though distance determinations. This method requires the bar length to be well measured, and that the CR lies exactly at the bar end, which is somewhat of an approximation. This method can give a wide range of bar pattern speeds from 35-60km s^{-1} kpc^{-1}(see Gerhard 2011).

Pattern speeds can also be measured by use of a stellar steaming method (Dehnen 2000; Quillen & Minchev 2005; Minchev et al. 2007). By measuring the tangental and perpendicular velocity components to a circular orbit in the Solar vicinity ($u - v$), and creating so-called velocity ellipsoids, models can be constructed to replicate the features. The pattern speed directly impacts the features seen in these ellipsoids, though it is not clear how to differentiate between the effect of the bar or the arms. Dehnen (1999) and Minchev et al. (2007) find approximate pattern speeds of 50km s^{-1} kpc^{-1} by inferring the position of the OLR.

One interesting method is to use ice age epochs here on Earth to determine the time of spiral arm passage. Ice ages correlate with cosmic ray strength. As the Earth passes into and out of a spiral arm, it experiences a differing amount of Galactic cosmic rays due to the greater net supernovae flux in the arm regions. Therefore peaks in cosmic ray fluxes are inferred as corresponding to Earth's passage through spiral arms, which allows for an estimate of arm pattern speed. Shaviv (2003) and Gies & Helsel (2005) use this method to infer an arm pattern speed of 14-17km s^{-1} kpc^{-1}.

It is somewhat more straightforward, if more time-consuming, to simply tailor numerical simulations to observations and thus infer the corresponding pattern speed (e.g. Rautiainen et al. 2008). This is simple to do for external galaxies, where the radial extent of features is expected to enclosed by the ILR/OLR which are in turn a direct result of the pattern speed. However, for the Milky Way this is again more complicated, and simulations must be tailored to some other observational constraint such as Oort constants, rotation curve, or l-v data. Modelling of velocity field by Chakrabarty (2007) suggest 58km s^{-1} kpc^{-1} for the bar, and find the arm speed is less well constrained. Modelling of the spiral and bar component and constraining to the l-v plot,

[12]The pattern speed is often in units of km s^{-1} kpc^{-1}, despite it being an angular frequency. 1km s^{-1} kpc^{-1} is equivalent to 0.001rad Myr^{-1}.

Bissantz et al. (2003) find a best fit bar speed of 60km s^{-1} kpc^{-1} and arm speed of 20km s^{-1} kpc^{-1}, though this is only done so for the inner disc ($R < 7$kpc). Simulations of gas flow inside a 2-armed potential by Martos et al. (2004) using a fine grid of pattern speeds find that 20km s^{-1} kpc^{-1} provides good dynamical consistency. Englmaier & Gerhard (1999) perform hydrodynamical simulations looking into the effect of different bar pattern speeds. They tend to favour values from 50-60km s^{-1} kpc^{-1}, corresponding to a bar co-rotation radius near 3.5kpc. They also include an armed potential, but assume it rotates with the bar. Fux (1999), Weiner & Sellwood (1999) and Rodriguez-Fernandez & Combes (2008) perform hydrodynamical simulations in the presence of a bar perturbation and attempt to match features in *l*-*v* observations. Collected together their best-fitting values span a wide range, with orientations of 20-40°and pattern speeds ranging from 30-50km s^{-1} kpc^{-1}.

In most of studies the arms and bars have been found to be rotating at very different pattern speeds, with the bar rotating up to three times as fast as the arms. This brings into question just how the two are related. If there are two distinctly different pattern speeds, then the arms need not necessarily be attached to the end of the bar. Indeed, this is not always the case in external galaxies also (e.g. NGC 1073, NGC 4548, NGC 5383). While there is some evidence for distinct pattern speeds in simulations (Sellwood & Sparke 1988) and external galaxies (e.g. Rautiainen et al. 2008; Gabbasov et al. 2009), if the pattern speed is measured as a function of radius it has been seen to be decreasing towards the outer disc (i.e. behaving as material arms) in some external galaxies (e.g. Speights & Westpfahl 2012; Meidt et al. 2008) and simulations (Grand et al. 2012; Baba et al. 2013). Needless to say, the true nature of arm and bar structures, including their origin, longevity and rotation rate, is still somewhat of an unknown.

1.7 Summary of Galactic structure

As can be seen by the previous sections, there is beginning to emerge some consensus on the spiral/bar structure, though there is still plenty of room for interpretation. With recent works there has emerged the idea that a 2-armed in stellar distribution could be driving 4-armed features in the gas, which goes some way of explaining the 2/4-armed dichotomy in the literature. The values of the arm pitch angles seem to lie between 10° and 25°, with the standard value approximately 13°. To put this into a galactic perspective, the pitch in external galaxies range from 4°to 20°, with Sa galaxies having a mean pitch angle of 6°whereas the Sc galaxies have a mean pitch angle of 18°(Russeil 2003). Studies of local material however tends to be highly dispersive, with a large amount of material lying away from spirals arms in the models. This could be because the Local arm is a separate entity to a grand design structure, or it could be that the Galaxy is better represented by a flocculent disc. Spirality appears to extend from $3 < R < 15$kpc, with the pitch angle potentially increasing in the outer disc. At least one bar appears present in the inner disc, but the already uncertain length, orientation, and rotation speed are only complicated by the suggestion of a second bar.

The pattern speeds of the arms and bar are also uncertain, though rough consensus tends to be that each rotates with a different speed. Past studies suggest arms in the outer disc appear to

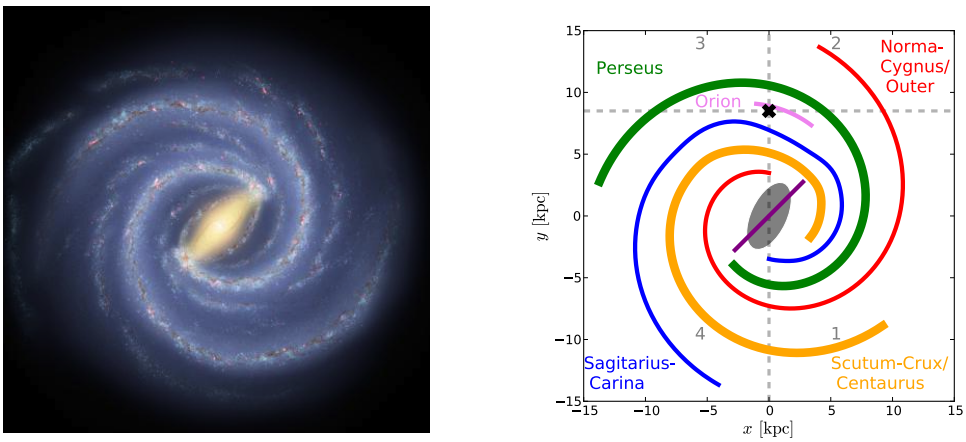

Figure 1.24: The current "standard" Milky Way morphology. The left panel shows an artist impression presented in Churchwell et al. (2009). The right panel is a schematic representation, showing locations of the primary spiral arm and bar features. The thick arms are stellar arms in 2:4, star:gas arm models and the thinner arms those primarily seen in gas. Two inner bars are shown, the spheroidal "boxy/peanut" bar ($\theta_b \approx 20°$) and the "Long" bar ($\theta_b \approx 45°$).

rotate about a third of the rate of the inner bar, though these values have large uncertainties.

The current "standard" artist interpretation of the Milky Way is shown in the left panel of Figure 1.24 taken from Churchwell et al. (2009). Beside which is a simple schematic of the arm and bar structures, modelled after a similar diagram in Benjamin (2008). The approximate locations of the four primary spiral arms are shown, with the density higher in the Scutum-Crux-Centaurus and Perseus arms compared to the others. In the centre the two possible bars are shown with differing orientation and lengths. Collating all of this together, the Milky Way is likely a SAB galaxy, similar in nature to NGC 1232, NGC 2336 and M61, which are each shown in Figure 1.25 for comparison. However, the reader must keep in mind that the evidence of the previous sections is effectively all that stands behind the illustration in Figure 1.24. It still seems like somewhat of a leap from the data in Figures 1.20, 1.21 and 1.22 to Figure 1.24.

1.8 Thesis aims

We propose to lift the veil on some of this confusion by performing a study to reproduce the *l*-*v* features of our Galaxy using numerical simulations of the Galactic ISM. The *l*-*v* distribution is unique in that it enables the tracing of spiral features separately without having to perform difficult distance determinations. A simulation is ideal as it contains all the spatial information, enabling for the simple reconstruction of a top-down distribution. We choose to primarily concentrate our efforts on reproducing the CO distribution, rather than H I, as it is a stronger tracer of spiral features, appearing in much denser regions of the ISM. While a similar approach has been attempted by some studies in the past, none has attempted to fully model all arm and bar parameters in depth, instead usually concentrating on constraining one or two values (e.g. bar pattern speed and orientation). We also utilise a radiative transfer scheme and chemical network to more closely model

Figure 1.25: A collection of Milky Way analogues from various sources. Note the multi-armed structure and short inner bar. UGC 12158 in Fig. 1.4 is also such a galaxy. Images are, from left, NGC 1232 (credit: ESO/IDA/Danish 1.5 m/R.Gendler & A. Hornstrup), M61 (credit: R. Gendler & R. Hannahoe) and NGC 2336 (credit: A. Block/Mount Lemmon SkyCenter/University of Arizona) inclined at approximately 60°.

the ISM emission.

There have been a number of previous numerical works aiming to reproduce *l*-*v* features. Lee et al. (1999) and Weiner & Sellwood (1999) observe the effect of a barred potential on a gas disc in the inner Galaxy, and projecting the gas particles into *l*-*v* space to match the observations. Similarly Rodriguez-Fernandez & Combes (2008) compare the *l*-*v* features of a number of bar models to observations, instead concentrating on matching the terminal velocity curves in the inner Galaxy. Bissantz et al. (2003) use arm and bar potentials to match *l*-*v* data, specifically investigating pattern speeds of each component. Baba et al. (2010) instead use the effect of an *N*-body model on a gas disc to match *l*-*v* features, varying the location of the observer somewhat in a single model. A key difference to our approach is to take into account the optical depth effects of the ISM by the use of a radiative transfer code. The aforementioned attempts at reproducing *l*-*v* structures simply re-project the positions and velocity of the gas into *l*-*v* space, taking no account of the relative strength of these features. The addition of a chemical network also allows for a direct tracing of CO gas, rather than simply assuming that high gas density corresponds to emission features in *l*-*v* space as done by the above studies. Previous studies also tend to focus on a single aspect of the Galaxy, such as pattern speed, or bar orientation. We instead aim to match all primary morphological features of the Milky Way; arm number, patterns speeds, pitch angles, bar orientations and allow for a variable observer position within the disc to thoroughly investigate the possible models. This requires a large number of models compared to the studies mentioned above, and at a reasonable resolution to allow for the sufficient formation of molecular gas.

Some key questions we intend on answering with this approach are:

- Can we create synthetic molecular emission maps of our own Galaxy sufficient for the purpose of constraining morphology?
- Can a grand design spiral perturbation sufficiently reproduce the observed features in *l*-*v* space (using a fixed potential)?
- Is a 2-armed structure sufficient to reproduce all the features, or is a 4-armed model needed?

- Does a 2-armed stellar distribution produce a 4-armed gas morphology sufficient to match *l*-*v* features?
- Can instead a transient spiral structure better fit the observations (using an *N*-body stellar system)?

While a full reproduction of all of the features seems unlikely due to the simplifications needed in any such treatment of a galactic-scale system, this thesis aims at narrowing the parameter space describing the morphology of the Milky Way, and eliminate some of the confusion in the many different, seemingly conflicting, paradigms.

The following chapters will be as follows. Chapter 2 will discuss the simulation technique and ISM specific physics required to model the molecular component of the Milky Way. Chapter 3 presents the results of simulations using fixed potentials for the arms and bar, and a simple method of addressing the uncertainty in the Earth's position and velocity. Chapter 4 describes the method of creating synthetic observations and the application to the calculations in the previous chapter, and the resulting best fit barred-spiral model of the Galaxy. Chapter 5 presents a similar study to that of the previous two chapters, but instead using an *N*-body prescription to model the stellar component of the Milky Way, rather than using fixed analytic potentials. We finish in Chapter 6 with a discussion of future work and conclusions to the work presented in this thesis.